Remote Sensing of Environment

Global estimates of surface albedo from Sentinel-3 OLCI and SLSTR data for Copernicus Climate Change Service: Algorithm and preliminary validation

--Manuscript Draft--

Manuscript Number:	RSE-D-22-01151
Article Type:	Research Paper
Section/Category:	Land surface reflectance and temperature (including sensor calibration studies)
Keywords:	albedo; algorithm; Sentinel-3; validation
Corresponding Author:	Jorge Sánchez-Zapero EOLAB SPAIN
First Author:	Jorge Sánchez-Zapero
Order of Authors:	Jorge Sánchez-Zapero
	Fernando Camacho
	Enrique Martínez-Sánchez
	Javier Gorroño
	Jonathan León-Tavares
	Iskander Benhadj
	Carolien Toté
	Else Swinnen
	Joaquín Muñoz-Sabater
Abstract:	The aim of Copernicus Climate Change Service (C3S) is to supply reliable climate data in support of strategies to adaptation and mitigation to climate change. The C3S provides access to high-quality climate data through its Climate Data Records (CDRs) of atmospheric, marine and land Essential Climate Variables (ECVs). Global Earth Surface Albedo (SA) satellite-based products are included in the land (biosphere) portfolio. SA is a magnitude which quantifies the fraction of solar energy reflected by the surface of the Earth. This paper details the retrieval methodology and preliminary validation results for global estimates of surface albedo based on Sentinel-3 observations for the C3S ECVs data (C3S SA v3.0). The retrieval algorithm incorporates measurements from the Ocean and Land Colour Instrument (OLCI) and the Sea and Land Surface Temperature Radiometer (SLSTR) on-board Sentinel-3 A and B satellites. Firstly, the atmospherically corrected reflectances are generated in the Copernicus Global Land Service framework. After that, the Bidirectional Reflectance Distribution Function (BRDF) inversion module concludes the BRDF model parameters, which are transferred to the angular integration module in order to generate spectral albedo quantities for the selected OLCI (Oa03, Oa04, Oa07, Oa17 and Oa21) and SLSTR (S1, S2, S5 and S6) bands. At the end, the spectral integration module generates broadband albedo quantities in three different standard broadband spectral regions (visible [[EQUATION]] , near infrared [[EQUATION]] and total shortwave [[EQUATION]]). Preliminary validation results over 10-months demonstration period (July 2018-April 2019) show, in terms of spatial and temporal consistency, that C3S Sentinel-3 SA global estimates reached in general good agreement as compared to other satellite operational references derived from MODIS (MCD43A3 C6) and PROBA-V (C3S PROBA-V SA v1.0) acquisitions. The comparison with ground data shows similar results to the MCD43A3 C6 comparisons but opposite sign in differences (marginally positive in case of Sentinel-3), with accuracy of 0.005 (3.7%), precision of 0.016 (11.3%) and uncertainty of 0.032 (22.7%). Our results have demonstrated the feasibility to estimate global fields of SA from Sentinel-3 observations, with similar quality than existing operational products. These Sentinel-3 based SA datasets will give the continuity to the existing C3S SA CDR, introducing improvements in terms of spatial resolution (300 m) and spectral information (9

	spectral albedos) in contrast to previous datasets based on Advanced Very High Resolution Radiometer (AVHRR; 4 km, 4 channels) and Vegetation instruments (VGT; 1 km, 4 channels).
Suggested Reviewers:	Zhuosen Wang University of Maryland Baltimore zhuosen.wang@nasa.gov expert in salbedo retrieval / CEOS LPV leader on albedo product validation area
	Alessio Lattanzio EUMETSAT alessio.lattanzio@eumetsat.int albedo development product expert at EUMETSAT
	Simon Blessing FastOpt GmbH simon.blessing@fastopt.de product development (LAI, FAPAR, ALBEDO) expert from optial satellite data
Opposed Reviewers:	

Retrieval method for global surface albedo estimates from Sentinel-3 is proposed.

Algorithm is based on BRDF inversion, angular and spectral integration.

A cross-comparison with MODIS and PROBA-V satellite products is performed.

The direct validation includes comparison with spatially representative ground data.

Global estimates of surface albedo from Sentinel-3 OLCI and SLSTR data for Copernicus Climate Change Service: Algorithm and preliminary validation.

Jorge Sánchez-Zapero [(1)(*)], Fernando Camacho [(1)], Enrique Martínez-Sánchez [(1)], Javier Gorroño [(1)], Jonathan León-Tavares [(2)], Iskander Benhadj [(2)], Carolien Toté [(2)], Else Swinnen [(2)], Joaquín Muñoz-Sabater [(3)]

(*) Correspondence: jorge.sanchez@eolab.es; Tel.: +34-963-769-448

(1) Earth Observation Laboratory (EOLAB), C/ Savina 8 – A4, 46980 Paterna (Valencia), Spain

(2) Flemish Institute for Technological Research (VITO), Remote Sensing Unit, Boeretang 200, B-2400 Mol, Belgium; iskander.benhadj@vito.be

(3) European Centre for Medium-Range Weather Forecasts (ECMWF), Shinfield Road, RG2 9AX, Reading, UK; joaquin.Munoz@ecmwf.int

Abstract

The aim of Copernicus Climate Change Service (C3S) is to supply reliable climate data in support of strategies to adaptation and mitigation to climate change. The C3S provides access to high-quality climate data through its Climate Data Records (CDRs) of atmospheric, marine and land Essential Climate Variables (ECVs). Global Earth Surface Albedo (SA) satellite-based products are included in the land (biosphere) portfolio. SA is a magnitude which quantifies the fraction of solar energy reflected by the surface of the Earth. This paper details the retrieval methodology and preliminary validation results for global estimates of surface albedo based on Sentinel-3 observations for the C3S ECVs data (C3S SA v3.0). The retrieval algorithm incorporates measurements from the Ocean and Land Colour Instrument (OLCI) and the Sea and Land Surface Temperature Radiometer (SLSTR) on-board Sentinel-3 A and B satellites. Firstly, the atmospherically corrected reflectances are generated in the Copernicus Global Land Service framework. After that, the Bidirectional Reflectance Distribution Function (BRDF) inversion module concludes the BRDF model parameters, which are transferred to the angular integration module in order to generate spectral albedo quantities for the selected OLCI (Oa03, Oa04, Oa07, Oa17 and Oa21) and SLSTR (S1, S2, S5 and S6) bands. At the end, the spectral integration module generates broadband albedo quantities in three different standard broadband spectral regions (visible $[0.4\mu m - 0.7\mu m]$, near infrared $[0.7\mu m - 4\mu m]$ and total shortwave $[0.3\mu m - 4\mu m]$). Preliminary validation results over 10-months demonstration period (July 2018-April 2019) show, in terms of spatial and temporal consistency, that C3S Sentinel-3 SA global estimates reached in general good agreement as compared to other satellite operational references derived from MODIS (MCD43A3 C6) and PROBA-V (C3S PROBA-V SA v1.0) acquisitions. The comparison with ground data shows similar results to the MCD43A3 C6 comparisons but opposite sign in differences (marginally positive in case of Sentinel-3), with accuracy of 0.005 (3.7%), precision of 0.016 (11.3%) and uncertainty of 0.032 (22.7%). Our results have demonstrated the feasibility to estimate global fields of SA from Sentinel-3 observations, with similar quality than existing operational products. These Sentinel-3 based SA datasets will give the continuity to the existing C3S SA CDR, introducing improvements in terms of spatial resolution (300 m) and spectral information (9 spectral albedos) in contrast to previous datasets based on Advanced Very High Resolution Radiometer (AVHRR; 4 km, 4 channels) and Vegetation instruments (VGT; 1 km, 4 channels).

1. Introduction

Surface albedo (SA), defined as the ratio of the radiant flux reflected from the Earth's land surface to the incident flux, is considered a terrestrial Essential Climate Variable (ECV) according to the Global Climate Observing System (GCOS) to characterize the state of the global climate system and its evolution resulting from natural and anthropogenic forcing (GCOS-154, 2011; GCOS-200, 2016). SA is both a forcing variable controlling the surface energy budget and a sensitive indicator of environmental changes including land degradation (Dickinson, 1995). As a corollary, it also determines the fraction of solar energy absorbed by the surface and transformed into heat or latent energy. Land SA is therefore a key variable for characterizing the energy balance in the coupled surface-atmosphere system and constitutes an indispensable input quantity for soil-vegetation-atmosphere transfer models (Stephens et al., 2015). Also worth noting, climate sensitivity studies with Global Circulation Models have confirmed the unsteady nature of the energy balance with respect to small changes in Surface Albedo (Amut et al., 2007; Henderson-Sellers and Wilson, 1983; Ollinger et al., 2008; Sellers et al., 1995).

The albedo quantity most relevant in terms of energy budget comprises the shortwave domain (SW [0.3μm, 4μm]), where the solar down welling radiation is more relevant (Gueymard et al., 2019). SW domain includes the visible (VI [0.4μm, 0.7μm]) and near-infrared (NIR [0.7μm, 4μm]. Actually, different definitions of satellite albedo products exist according to the domain of directional integration (Schaepman-Strub et al., 2006): the directional-hemispherical reflectance (DHR) or black-sky albedo (BSA or AL-DH), and the bi-hemispherical reflectance (BHR) or white-sky albedo (WSA or AL-BH). BSA is defined as the ratio of the radiant flux for light reflected by a unit surface area into the view hemisphere to the illumination radiant flux, when the surface is illuminated with a parallel beam of light from a single direction (Lucht et al., 2000). On the other hand, WSA is the ratio of the radiant flux reflected from a unit surface area into the whole hemisphere to the incident radiant flux of hemispherical angular extent (Shuai et al., 2020). Combining BSA and WSA in relation to the proportion of sky irradiance, the blue-sky albedo is obtained, which is the actual albedo value (Lewis, P & Barnsley, 1994).

The Climate Change Service (C3S, https://climate.copernicus.eu/) of Copernicus European Union's Earth Observation (EO) programme aims to provide key indicators on the drivers of climate change, combining climate observations with the most recent science to develop and deliver quality guaranteed information about the past, current and future climate conditions in Europe and in the whole worldwide. In response to GCOS, the C3S produces Climate Data Records (CDRs) of many ECVs, including land SA. In the C3S, three broadband quantities are provided (visible, NIR, total shortwave) in both angular integration domains (black-sky and white-sky albedos). The existing C3S SA CDR, available in the Climate Data Store (CDS, https://cds.climate.copernicus.eu/#!/home) is based on past EO satellites time series, retrieved from the National Oceanic and Atmospheric Administration / Advanced Very High Resolution (NOAA/AVHRR) (Apr 1981- Dec 2005, at 4 km), Satellite Pour l'Observation de la Terre / Vegetation (SPOT/VGT) (Dec 1999 - May 2014, at 1 km) and Project for On-Board Autonomy Vegetation (PROBA-V) (Dec 2013 – Jun 2020, at 1 km). The continuity of the service can be ensured thanks to the switch to measurements from Ocean and Land Colour Instrument (OLCI) and Sea and Land Surface Temperature Radiometer (SLSTR) on-board ESA Sentinel-3 A (S3A) and B (S3B) satellites (Mecklenburg et al., 2018).

A rigorous approach for SA determination from EO top-of-atmosphere (TOA) data consists in solving the radiative transfer problem in the coupled surface-atmosphere system simultaneously (Betts, 2009). Such method was adopted in both algorithms to retrieve SA from both MISR (Diner et al., 2008, 1998) and Meteosat (Govaerts et al., 2008; Pinty et al., 2000a, 2000b) instruments. Other methods are based on TOA reflectances direct conversion to broadband SA without performing atmospheric correction (Liang, 2003). A robust and pragmatic approach for surface albedo determination distinguishes different steps in the processing chain (i.e., cloud masking and atmospheric correction, BRDF inversion, spectral albedo calculation, and narrow-to-broadband albedo conversion), and treats them independently. The spectral top-of-canopy (TOC) reflectance values serve as the input quantities for the inversion of a linear kernel-driven Bidirectional Reflectance Distribution Function (BRDF) model, which allows taking into account the angular dependence of the reflectance factor (Barnsley et al., 1994; Hu et al., 1997; Roujean et al., 1992; Wanner et al., 1995).This approach for retrieving surface albedo products was firstly included in the Polarization and Directionality of the Earth's Reflectances (POLDER) (Leroy et al., 1997) processing chain, then in Moderate Resolution Imaging Spectroradiometer (MODIS) MCD43 (Schaaf et al., 2002; Strahler et al., 1999), Spinning Enhanced Visible and InfraRed Imager (SEVIRI) (Carrer et al., 2010; Geiger et al., 2008), AVHRR (Lellouch et al., 2020), andadapted to Vegetetion sensors in C3S (Carrer et al., 2021) afterwards. This robust approach was selected in the first albedo retrieval algorithm implementation using Sentinel-3 data in the framework of the C3S (named as C3S SA v3.0) as gives a good compromise between simplicity of implementation, computation time and quality of the outputs. This explains why it is widely used in operational contexts, such as NASA MODIS (https://modis.gsfc.nasa.gov/), the Satellite Application Facility for Land Surface Analysis (LSA SAF, https://landsaf.ipma.pt/en/) program of EUMETSAT or the Copernicus Global Land Service (CGLS, https://land.copernicus.eu/global/index.html).

On the other hand, a framework for the Evaluation and Quality Control (EQC) of climate data products derived from satellite and in situ observations was developed within the C3S CDR (Nightingale et al., 2019). Validation, or quality assessment, is one of the main components defined in this EQC framework, and it is defined as the process of independently assessing the quality of the data products derived from the system outputs (Justice et al., 2000). Scientific quality assessment is necessary to ensure the compliance of the products to user requirements, and C3S SA v3.0 demonstration products underwent a scientific evaluation before they are realised to the users.

The validation methodology follows the good practices recommended by the Land Product Validation sub-group (LPV, https://lpvs.gsfc.nasa.gov/) of the Working Group on Calibration and Validation (WGCV) of the Committee on Earth Observing Satellites (CEOS) for the validation of satellite-derived global albedo products (Wang et al., 2019). The validation strategy includes two different approaches, the direct and indirect validation. The direct point-to-pixel validation (i.e. direct validation) consists of satellite products comparisons with albedo measured from in situ tower-based instruments (Lewis, P & Barnsley, 1994). Direct validation enables the assessment of uncertainties, and it may be argued that only such methods can be seen as actual validation in the field of remote sensing (Mayr et al., 2019). Product-to-product validation approach refers to the intercomparison of satellite products (i.e., indirect validation), which allows the evaluation of discrepancies (systematic or random) between products and relative uncertainties. Indirect validation is very helpful to compute metrics that cannot be obtained with ground measurements for the limitations in terms of representativeness and global conditions. However, indirect validation does not provide absolute validation results, since satellite products intercomparison alone are not enough to validate new products.

This paper describes the algorithm and preliminary validation results over a demonstration period of 10 months (July 2018-April 2019) of the SA retrieval algorithm based on Sentinel-3 OLCI and SLSTR data, developed in the framework of the C3S. The paper is structured as follows: Sections 2 and 3 describe the input datasets and validation methodology respectively; section 4 presents the albedo retrieval algorithm, section 5 presents the quality assessment results while conclusions are summarized in section 6.

2. Data

2.1. Sentinel-3 input data

2.1.1. Characteristics of Sentinel-3 OLCI and SLSTR instruments

As part of the Copernicus programme, Sentinel-3 is the third of the Sentinel satellite series, originally dedicated to ocean and land applications including sea-ice, water quality monitoring in open-ocean, coastal and inland areas, surface temperature, sea height, and vegetation productivity. The mission provides continuity to the observations from Envisat space-borne missions. The first platform, Sentinel-3 A, has been flying since 16 February 2016. The second platform, Sentinel-3 B, was successfully launched on 25 April 2018. Sentinel-3 is a Low Earth Orbit (LEO), with a mean altitude of 815 km and sun-synchronous, and a local equatorial crossing time of 10:00 am.

OLCI (https://sentinels.copernicus.eu/web/sentinel/user-guides/sentinel-3-olci) is one of the four instruments present on the Sentinel-3 platform. As a continuity of the Envisat MEdium Resolution Imaging Spectrometer (MERIS), OLCI is a push-broom imaging spectrometer that measures solar radiation reflected by the Earth in 21 spectral bands encompassed in visible and NIR, with a high spatial resolution of 300 m at the nadir view, and a swath width of 1270 km. It includes five camera modules; the field of view (FOV) of each camera is arranged in a fan-shaped configuration in the vertical plane perpendicular to the platform velocity. Each camera has an individual FOV of 14.2 degrees with a 0.6 degree overlap with its neighbours to cover a wide 68.5 degree across-track FOV.

SLSTR (https://sentinels.copernicus.eu/web/sentinel/user-guides/sentinel-3-slstr) is a conical scanning imaging radiometer employing the along-track scanning dual-view technique to measure the radiance at the top of the atmosphere in nine spectral channels: six solar channels from the visible (554 nm) to the Short Wave-Infrared (SWIR) (3.74 μm), and two in the thermal infrared (10.85 and 12.02 μm). Each scene is observed twice: in nadir and backwards views. SLSTR is an evolution of the Along Track Scanning Radiometer (ATSR) series and Advanced Along Track Scanning Radiometer (AATSR) with a wider swath (1420 km in nadir, 750 km in backwards view) and an increased spatial resolution (~500 m).

2.1.2. Pre-processing of Sentinel-3 OLCI and SLSTR data

Atmospherically corrected reflectances derived from OLCI and SLSTR observation on-board of Sentinel-3 A and B satellites (PDGS, 2016) are the input for SA retrieval algorithm. These TOC reflectances are brokered from CGLS Sentinel-3 pre-processing chain, which is common to all Sentinel-3 based CGLS biophysical variables. TOC reflectances are retrieved from Level 1B Sentinel-3 TOA radiometry following the next steps: collocation and reprojection of OLCI and SLSTR Level 1B input on the regular 300 m plate carrée grid using the S3-MPC SYN_L1C tool (https://github.com/bcdev/l1c-syn-tool); ii) cloud, cloud shadow and snow classification based on the OLCI Identification of Pixel (IdePix) propierties algorithm (S3_MPC, 2019) and the SLSTR summary cloud flag (S3_MPC, 2021a); and iii) Atmospheric Correction (Ramon et al., 2021) based on the Simplified Method for Atmospheric Correction (SMAC) (Rahman and Dedieu, 1994).

The Atmospheric Correction (AC) was evaluated in the CGLS (Jolivet, 2021) following the AC intercomparison exercise approach (Doxani et al., 2018). The comparison of TOC reflectances with reference products show accuracy variability, depending on the spectral channel, from 10^{-3} to 1.2 10^{-2} and precision and uncertainty from 0.012 to 0.033. Reference product was retrieved using an accurate radiate transfer code and inversion of the in-situ Aerosol Robotic Network (AERONET) products for aerosols optical thickness and model.

The internal CGLS quality assessment of Sentinel-3 TOC reflectances (Sánchez-Zapero et al., 2021b) demonstrated reliable performance at global scale and spatially accordance with Sentinel-2 at local study cases. OLCI and SLSTR equivalent channels showed good consistency and similar temporal trends. The comparison with Radiometric Calibration Network (RadCalNet) in-situ measurements over four different sites showed also good temporal consistency. The comparison of OLCI and SLSTR equivalent channels TOC retrievals over selected local cases of interest (representatives of different biome types) showed also good agreement (positive bias < 5%). Observations over desert calibration sites (Lacherade et al., 2013) from different satellites (S3A versus S3B) were found also consistent: bias indicator typically <1% while uncertainty and precision around 10%. The comparison with Radiometric Calibration Network (RadCalNet) in-situ measurements over four different sites showed good temporal agreement and positive bias, with median deviation (accuracy) lower than 3% (tipically) and large differences in the OLCI and SLSTR lower channels. However, large negative differences were found in the comparison of SLSTR S5 and S6 channels against RadCalNet, that could be reduced applying the vicarious calibration coefficients (from -11% to -1% in S5, from -18% to 4% in S6). In summary, the quality assessment demonstrated the reliability and suitability of Sentinel-3 TOC reflectances to produce biophysical products. The main limitations come from the ancillary quality layers (cloud masking and error characterization) and the underestimation in the SWIR region (S5 and S6 SLSTR channels) (S3_MPC, 2021b).

CGLS includes a total of 20 spectral bands of Sentinel-3 TOC reflectances (15 from OLCI and 5 from SLSTR). In this version of the Sentinel-3 surface albedo retrieval algorithm, the bands that provide less information, predominate in highly sensitive areas or are spectraly redundants (i.e., SLSTR and OLCI overlap) were discarded. Table 1 summarizes the information of the 9 selected bands (central wavelength and width) used as the input in the Sentinel-3 SA algorithm.

Table 1: Characteristics of Sentinel-3 OLCI (Oa03, Oa04, Oa07, Oa17, Oa21) and SLSTR (S1, S2, S5, S6) channels used as input of the surface albedo retrievals.

Spectral band	Oa03	Oa04	Oa07	Oa17	Oa21	S1	S2	S5	S6
λ centre (nm)	442.5	490	620	865	1020	554.27	659.47	1613.4	2255.7
Width (nm)	10	10	10	20	40	19.26	19.25	60.68	50.15

A well-known limitation of the IdePix cloud/snow algorithm is the misidentification of snow and clouds (Toté, 2020), removing most of snow observations when all the IdePix cloud flags (i.e., "cloud", "cloud_ambiguous", "cloud_buffer", "cloud_shadow") are applied. Consequently, an alternative decision rule based on Normalized Difference Snow Index (NDSI) threshold in combination with less restrictive IdePix flags (i.e., "cloud", "cloud_ambiguous") has been implemented to identify pixels likely associated with snow. The NDSI was computed using green (S1) and SWIR (S5) SLSTR spectral bands. A threshold of 0.42 (https://sentinels.copernicus.eu/web/sentinel/technical-guides/sentinel-2-msi/level-2a/algorithm) was found useful to identify snow pixels from Sentinel-3 (Figure 1). For snow-free pixels (NDSI<0.42) the additional two cloud flags ("cloud_shadow", "cloud_buffer") were applied.

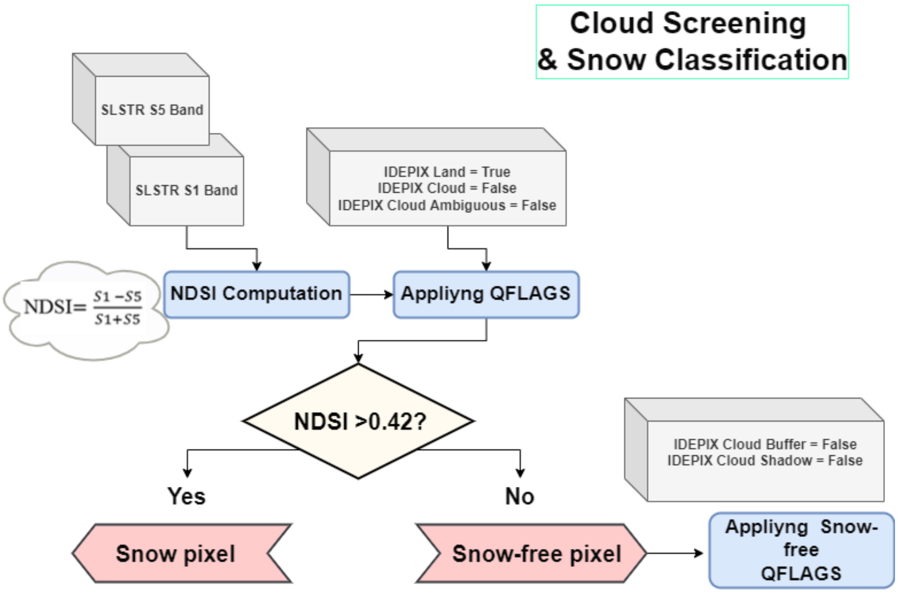

Figure 1: Diagram for cloud screening and snow classification.

2.2. Validation data

2.2.1. Ground measurements

A careful selection of best in-situ reference albedo measured from tower-based instrument is mandatory for the comparison with satellite albedo products. For a meaningful point-to-pixel comparison, it is crucial the good characterization of the spatial representativeness around the ground-based measurements. Homogeneous sites were selected showing similar footprints than satellite pixel resolutions of interests. 58 stations (see Annex I) were taking into account in the evaluation of the spatial representativeness: 17 sites come from the CGLS Ground-Based Observations for Validation (GBOV, https://gbov.acri.fr/, which collects data from other existing networks such as ESRL GMD, SURFRAD, BSRN, FLUXNET and OZFLUX), 25 from the National Ecological Observatory Network (NEON, https://www.neonscience.org/), 4 from the Integrated Carbon Observation System (ICOS, https://www.icos-cp.eu/) and 12 from The Environmental Resources Network (TERN, https://www.tern.org.au/). Most of them (33 sites) are considered 'Super Sites' endorsed by the CEOS LPV, as they are deeply characterized in terms of bio-geophysical variables and canopy structure and have infrastructural capacity to keep active in long-term operations.

The spatial representativeness was evaluated at 1 km. The methodology, adopted from CEOS LPV recommendations, is based on the estimation of geostatistical indexes (Román et al., 2010, 2009), comparing the variogram model parameters obtained at different spatial resolutions (1 km - 1.5 km). Four geostatistical attributes were procured from variogram model parameters (Cescatti et al., 2012; Román et al., 2010): relative strength of the spatial correlation (R_{ST}), relative coefficient of variation (R_{CV}), scale requirement index (R_{SE}), and relative proportion of structural variation (R_{SV}). Combining the four geostatistical attributes it is generated the standard score (ST_{SCORE}, a score of spatial representativeness which use R_{SE} as more weighted marker and the others like secondary markers (see Eq. 1). In cases when semi-spherical variogram model does not provide a good fit to the variogram estimator, the first order score (RAW_{SCORE}) could be used to provide a mark of the spatial representativeness (Eq. 2), less recommended due to are only based on the R_{CV}.

$$\mathrm{ST_{score}} = \left(\frac{|R_{CV}|+|R_{ST}|+|R_{SV}|}{3} + R_{SE}\right)^{-1} \qquad \text{Eq. 1}$$

$$\mathrm{RAW_{score}} = |2\ \mathrm{R_{CV}}|^{-1} \qquad \text{Eq. 2}$$

Both, ST and RAW scores are directly proportional to site spatial homogeneity or representativeness. It is proposed to use a score threshold of 2.0 in ST_{SCORE} to decide which one is a homogeneous or spatially representative site as large differences are expected for sites below to this threshold (Cescatti et al., 2012; Sánchez-Zapero et al., 2020). In case where ST_{SCORE} cannot be computed, same threshold of 2.0 in RAW_{SCORE} was used.

Finally, 33 sites were considered homogeneous or spatially representative for the comparison of satellite products at 1 km resolution (see Annex II, where a summary of the main geostatistical attributes for each selected site used in accuracy assessment at 1km resolution is presented). The ground stations are grouped according to the main biome types (27 forest, 4 grasslands, 1 croplands and 1 bare area). Note that *USA_GCMK, KONZ, ORNL, MLBS, STEI, AU_Cum* and *AU_GWW* are not considered representative at 1km resolution during the leaf-on season and *USA_PSUS and USA_SFSD* during the leaf-off season. Additionally, *USA_NRFT, BONA* and *DEJU* were not used in the leaf-off season period due to not clear images were found in the period to analyze the representativeness of the site due to persistent cloudy or snow events.

2.2.2. Satellite products

In this section, the main characteristics of SA products involved in the quality assessment are described (Table 9). MODIS BRDF/Albedo (MCD43A3) Collection 6 (C6) (Schaaf and Wang, 2015) and C3S PROBA-V SA v1.0 (Carrer et al., 2019) products are used as a reference. They have reached CEOS LPV validation stage level three (Wang et al., 2018), as products are evaluated over global conditions and validation procedures followed community-agreed good practices. C3S PROBA-V SA v1.0 validation results (Sánchez-Zapero, 2019) showed systematic overestimation (11.5%) compared with 20 homogeneous GBOV sites (2014-2018 period), mainly over forest sites for lower albedo ranges (SA < 0.2) (Sánchez-Zapero et al., 2020). MCD43A3 C6 showed better accuracy and opposite sign of differences (negative bias of -5.9%). Both reference products showed similar uncertainty (RMSD ~ 0.4) in comparison with GBOV data over homogeneous sites.

Equivalent spatial and temporal support sampling support must be defined for intercomparison of satellite products. The comparison was performed at 1 km spatial support area, which is the spatial resolution of PROBA-V SA products. For that, Sentinel-3 (300m resolution) average values in a 3x3 pixels window and 2x2 pixels for MCD43A3 C6 (500m resolution) were calculated. Previously, MCD43A3 C6 products were re-located in Plate Carrée projection. Furthermore, as C3S products temporal frequency is 10-days, it was selected as common temporal support period.

The Quality Flag information (Table 3) was applied to discard retrievals which have been flagged as low quality in case of reference product. For C3S SA v1.0 products, land pixels which show input status invalid or out of range and/or saturation in blue and red channels were discarded. In case of MODIS C6, pixels with best quality (i.e., magnitude inversion with number of valid observations of at least 7 days) and good quality (full inversion) were considered for the re-sampling over C3S spatial grid.

Table 2: Features of the global remote sensing SA products involved in the quality assessment.

Product	Satellite /Sensor	BRDF Model: Volumetric /Geometrical Kernels	Spatial resolution /Projection	Frequency /Composite period	Period available	Reference
C3S SA v3.0	Sentinel-3 /OLCI & SLSTR	Ross_Thick /Li_Sparse_Reciprocal	1/336° (~300m) /Plate Carrée	10 days /20 days (recursive using BRDF MODIS climatology).	July 2018 – April 2019	(Sánchez-Zapero et al., 2021a)
C3S SA v1.0	PROBA /VEGETATION	Ross_Thick /Roujean	1/112° (~1km) /Plate Carrée	10 days /30days	2014 – June 2020	(Carrer et al., 2019)
NASA MCD43A3 C6	TERRA+AQUA /MODIS	Ross_Thick /Li_Sparse_Reciprocal	500m /Sinusoidal	Daily /16days	2000 - present	(Schaaf and Wang, 2015),

Table 3: Summary of the quality flags used to discard invalid or low quality pixels.

Product	Quality Control Flag
C3S PROBA-V SA v1.0 QFLAG	Sea (bit 1) Input status out of range or invalid (bit 6) Saturation in Red (bit 10) and blue (bit 11) channels
MCD43A2 C6	BRDF Albedo Band Quality Bands 1 to 7: Magnitude inversion (number of observations lower than 7)

3. Validation Methods

The methods for quality assessment follow the CEOS LPV good practice protocol for the validation of satellite-derived albedo products (Wang et al., 2019).

For direct validation purposes, the in-situ albedometer footprints were tested in terms of spatial representativeness at the satellite evaluated pixel resolution, in concordance with tower-based measurements standards (Román et al., 2010, 2009) (see section 2.2.1). The next step involves the computation of satellite blue-sky albedo (Lewis, P & Barnsley, 1994) to compare ground measurements (direct validation). For that, the proportion of direct and diffuse down-welling shortwave radiation measured at the station is used to weight the corresponding BSA and WSA satellite best quality retrievals (Table 3). The average ground data values during the temporal composite window of satellite product (see Table 2) were computed were computed for the comparison. Furthermore, since satellite products provide BSA estimations at the Solar Local Noon (SLN), ground measurements have been chosen at SLN, too.

The product intercomparison approach is evaluated over LAND VALidation (LANDVAL) 720-site network. This selection of sites is representative of the global variability of land surface types (Fuster et al., 2020; Sánchez-Zapero et al., 2020).

The temporal consistency is evaluated through qualitative inspection of temporal trajectories. The error is quantitatively characterized assessing the Accuracy, Precision and Uncertainty (APU) metrics (see Table 4), reporting the goodness of fit between the evaluated dataset and the corresponding reference. They are adopted from experimental recommendations of Joint Committee for Guides in Metrology (JCGM) to the expression of uncertainty in measurement (JCGM-GUM, 2008) and from GCOS (GCOS-154, 2011). In addition to APU metrics, other statistics including linear model fits or correlation between datasets are used to evaluate the goodness of fit. Major Axis Regression (MAR) was chosen as linear fit model instead of Ordinary Least Squares (OLS) due to MAR is particularly conceived to handle error in both variables (x- and y-axis) (Harper, 2014).

The quality assessment of the C3S Sentinel-3 SA v3.0 satellite products is performed for a global test dataset covering the period from June 2018 to April 2019.

Table 4: Validation metrics.

Statistics	Comment
N	Number of samples. Indicative of the power of the validation
B	Mean Bias. Difference between average values of x and y. Indicative of accuracy and offset. Bias (%) is the relative mean bias between the average of x and y.
MD	Median deviation between x and y. CEOS LPV good practice reporting the accuracy. MD (%) is the relative MD between the average of x and y.
STD	Standard deviation of the pair differences. Indicates precision. STD (%) is the relative STD between the average of x and y.
MAD	Median absolute deviation between x and y. CEOS LPV good practice.MAD (%) is the relative MAD between the average of x and y.

RMSD	Root Mean Square Deviation. RMSD is the square root of the average of squared errors between x and y. CEOS LPV good practice reporting uncertainty. RMSD (%) is the relative RMSD between the average of x and y.
R	Correlation coefficient. Indicates descriptive power of the linear accuracy test. Pearson coefficient is used.
MAR	Slope and offset of the Major Axis Regression (MAR) linear fit. Indicates some possible bias
Conformity test	Percentage of pixels matching the user requirements (Table 6).

For the conformity testing, a review of a user uncertainty requirements (Table 5) collection was done. C3S, GCOS (GCOS-154, 2011) and World Meteorological Organization (WMO, https://space.oscar.wmo.int/variables/view/earth_surface_albedo) requisites are considered.

Table 5: Review of uncertainty requirements (GCOS, WMO and C3S SA).

GCOS	WMO	C3S
Max (5%; 0.0025)	Goal: 5% Breakthrough: 10% Threshold: 20%	Max (10%; 0.01)

Three different conformity levels (i.e., optimal, target and threshold) based on the existing requirements are predefined (Table 6), aiming at verifying whether the results are fit for validation purpose. The optimal level (Max [5%, 0.0025]) corresponds to the GCOS uncertainty requirement (which is partly equivalent to WMO goal level). The target level (Max [10%, 0.01]) is selected according to the C3S key performance indicator (KPI) (which is partly equivalent to the WMO breakthrough level). Lastly, the threshold level (Max [20%, 0.02]) is more similar to WMO threshold level. When products performances are above threshold level, it is considered as suboptimal quality.

Table 6: Predefined levels for unciertainty requirements used in the SA validation.

	Optimal	Target	Threshold
Surface Albedo Uncertainty Requirements	Max [5%, 0.0025]	Max [10%, 0.01]	Max [20%, 0.02]

4. Sentinel-3 albedo retrieval algorithm

4.1.1. Overview

The proposed Sentinel-3 SA retrieval approach flow diagram is described in Figure 2. It starts from TOC reflectances, which are generated in the CGLS service. The BRDF inversion and the albedo calculation (which involves angular and spectral integration) are constructed in the context of the C3S, and described in the following sections, being the outputs the spectral and broadband albedos (and associated uncertainties), delivered every 10 days (3 per month).

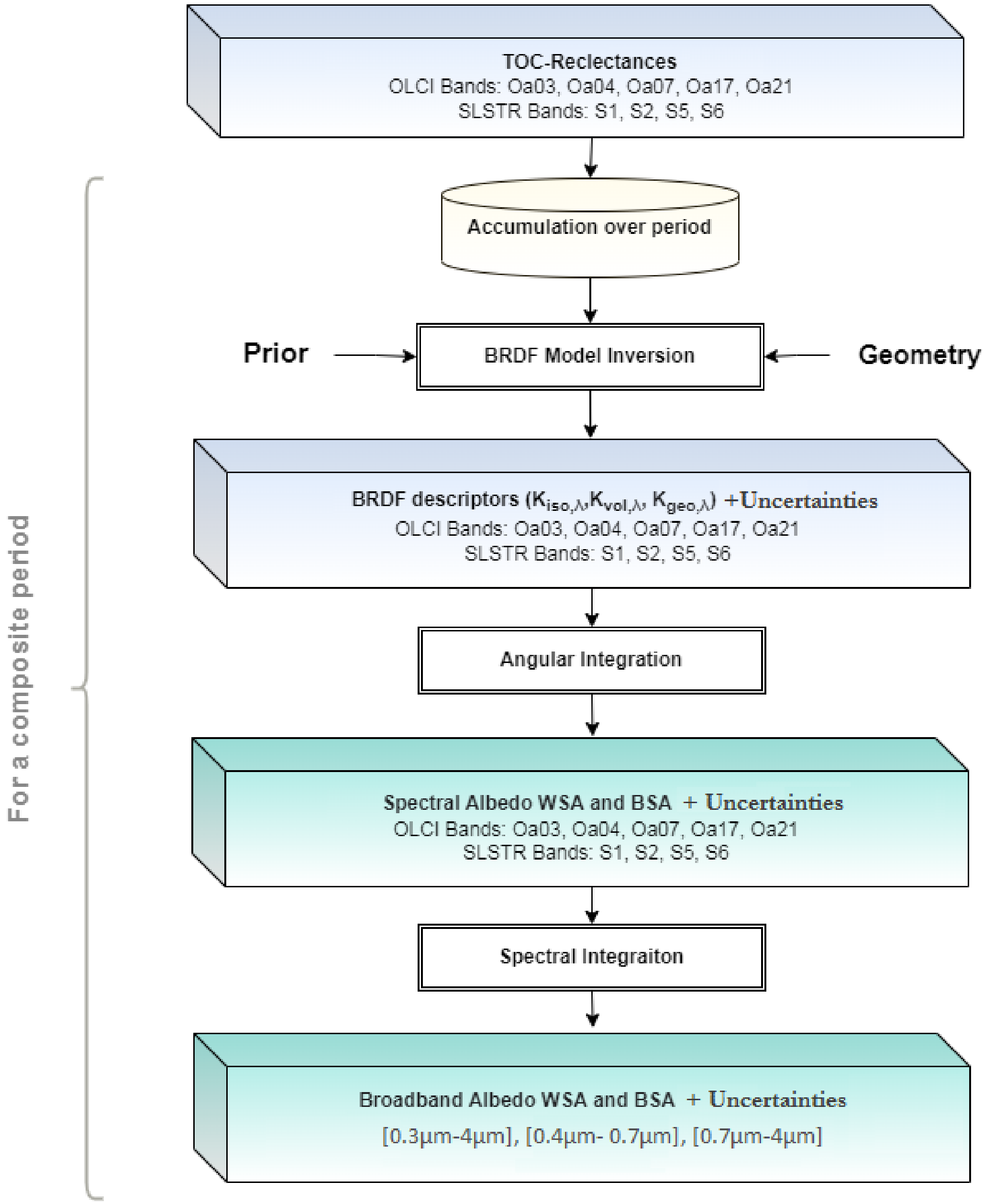

Figure 2: Flow diagram of the SA retrieval algorithm.

4.1.2. BRDF descriptors retrieval

Land Surface reflectance values depend on the spectral wavelength, as well as on different conditions in terms of observation, illumination and geometry (sensor and Sun locations). The BRDF, which quantifies the anisotropy of the reflectance, can be approximated by numerical inversion of kernel-driven semi-empirical models (e.g. RossThick-LiSparseReciprocal) making use of three parameters called BRDF descriptors or parameters (Roujean, 2017). It is now widely accepted that kernel-driven semi-empirical BRDF models can adequately represent the directional signature of most natural targets (Breon and Maignan, 2017; Bréon and Vermote, 2012; Claverie et al., 2015; Franch et al., 2014; Los et al., 2005; Lucht et al., 2000; Roujean et al., 1992, 2018; Roy et al., 2016; Schaaf et al., 2002; Vermote et al., 2009; Wanner et al., 1995). In the framework of C3S, the Regularised BRDF inversion for land surface reflectance (ReBeLS) processor, initially developed within CGLS (Leon-Tavares, 2020), was used to retrieve the BRDF model from Sentinel-3 surface reflectance data for the required OLCI and SLSTR channels (see Table 1).

ReBeLS starts with the ingestion of TOC reflectances, their associated geometries (solar viewing/azimuth, viewing and viewing azimuth angles), pixel quality flags and priors auxiliary data. The priors were built from climatology of MCD43 BRDF descriptors (Strahler et al., 1999) and are used as auxiliary information for the optimization of the BRDF inversion process (Muller et al., 2011). Layers are accumulated over a predefined period of time (for this version of the algorithm, 30 days and 365 days for near-real time (NRT) and back processing products, respectively).

The next step is the BRDF modelling, where kernels from a semi-empirical BRDF model are computed for each observation. ReBeLs uses the Roujean (Roujean et al., 1992) and RossThick-LiSparse (Wanner et al., 1995) models, which are the most popular kernel-driven semi-empirical models to approximate the BRDF of land surface, adopted in the operational data processing system of the MODIS MCD43 products and other operational chains ((Baret et al., 2013; Geiger et al., 2008; Lucht et al., 2000; Roujean et al., 2018; Schaaf et al., 2002). Finally, the BRDF inversion is performed, and BRDF descriptors that best represent the ensemble of observations are found by solvind an inverse problem (Geiger et al., 2008; Pokrovsky et al., 2003; Roujean et al., 2018) with the addition of regularisation (prior) (Quaife and Lewis, 2010).

The outputs of the BRDF model inversion stage are the retrieved RossThickLiSparse BRDF descriptors ($k_{iso}, k_{vol}, k_{geo}$) and their respective variances ($\sigma^2{}_{k_{iso}}, \sigma^2{}_{k_{vol}}, \sigma^2{}_{k_{geo}}$). An output control is also performed, and a quality information layer is assembled to reflect availability of observations and whether (or not) the BRDF model inversion was successful

4.1.3. Angular integration (spectral albedo)

For albedo calculation, the BRDF angular integration over all viewing angles is needed. Then, the spectral albedo values can be estimated by computing an angular integral of the kernel functions (f_i), once the BRDF descriptors are known (k_i). The algorithm estimates the black-sky and white-sky albedos to each sensor channel (Table 1) separately. BSA is the albedo over only direct illumination component (any diffuse component) and is function of the solar zenith angle. The BSA is computed at local solar noon. WSA is the albedo only comprised of isotropic diffuse illumination (in absence of direct component). As BSA is not affected by atmospheric scattering, WSA is variable with the intrinsic coupling between the surface and the scattering atmosphere. Instead of directly calculating the integrals of BSA and WSA, the same pragmatic method of polynomial representation of the BSA and WSA integrals proposed in the MODIS albedo estimating procedure (Strahler et al., 1999) is used.

SLSTR SWIR radiometry channels are known to suffer high radiometry calibration inaccuracies, which are translated to Sentinel-3 TOC reflectances brokered from CGLS. To correct adequately the measured radiance, vicarious calibration exercises have been performed and multiplicative corrections are strongly advised to be applied (S3_MPC, 2021b). Therefore, ESA post launch vicarious calibration coefficients proposed by the Sentinel-3 Mission Performance Centre (correction factors in SWIR domain of 1/1.1 and 1/1.13 for S5 and S6 SLSTR channels) were directly applied in the computation of spectral albedos.

4.1.4. Spectral integration (broadband albedo)

The integral of spectral albedos over a defined wavelength interval domain weighted by the spectral irradiance results in broadband albedo quantities (Liang, 2001). Most studies calculate broadband albedos by linear combination of available spectral albedo values in each spectral channel (Geiger et al., 2008; Liang, 2001; Liang et al., 2003; Van Leeuwen and Roujean, 2002) due to the approximation of the integral as a weighted sum of the integrand at discrete values of the integration variable. Then, the broadband albedo estimates (a_γ) for a certain spectral interval ($\gamma = [\lambda_1, \lambda_2]$) can be computed using a linear transformation of the spectral albedo values (a_λ) following the expression:

$$a_\gamma = c_{0\gamma} + \sum_j (c_{\lambda\gamma} a_\lambda) \qquad \text{Eq. 3}$$

were $c_{0\gamma}$ and $c_{\lambda\gamma}$ refer to the linear combination coefficients.

For the C3S SA v3.0 products, a different assemblage of coefficients was produced for both snow scenes and snow-free targets in three different broadband spectral domains: visible (VI - $[0.4\mu m - 0.7\mu m]$), near infra-red (NI - $[0.7\mu m - 4\mu m]$) and total shortwave (SW - $[0.3\mu m - 4\mu m]$).

The methodology to generate the combination coefficients applies a linear regression over a dataset of reference spectral albedo versus its respective broadband albedo. Both spectral and broadband albedo are acquired from a database of simulated/measured spectral albedo and radiative transfer simulations of downwelling irradiance.

For the generation of the linear combination coefficients, the linear regression is trained considering global representativeness of atmospheric and surface properties at global scale (i.e., a weighted linear regression). The global representativeness of the land surfaces has been achieved by extracting the data information from the global land cover classification GLC2000 (Bartholome and Belward, 2005). The aggregation per main biome was performed into 10 different classes, and the weights in the linear regression for the generation of narrow to broadband coefficients are proportional to the land surface area they represent at a global scale (see Table 7).

Table 7: Approximate percentage area of the Earth represented by the majority of 10 biome types.

Land Class	% Land area	Land Class	% Land area
Evergreen Broadleaved Forest	6.85	Grass	9.34
Deciduous Broadleaved Forest	7.05	Crop	15.85
Needle-Leaf Forest	15.22	Bare	13.08
Other	7.66	Snow	2.54
Shrub	22.20	Urban	0.20

The spectral albedo simulation uses PROSAIL (PROSPECT + SAIL) model, which combines the SAIL canopy level bidirectional (Scattering by Arbitrarily 82 Inclined Leaves; (Verhoef, 1984)) and the PROSPECT leaf spectral (Jacquemoud and Baret, 1990) models. Canopy reflectances in the radiation spectrum (400 – 2500 nm) at 1nm (Jacquemoud et al., 2009) are simulated using PROSAIL model. The model is run to simulate the directional-hemispherical and bi-hemispherical reflectances. Forest areas are simulated running PROSAIL due to is the most appropriate model to reproduce complex canopies. Therefore, the albedo for Deciduous Broadleaf (DBF), Needle-Leaf (NLF) and Evergreen Broadleaf (EBF) Forest biomes are generated using this method. The use of the PROSAIL radiative cannot be extended to describe any complex surface such as bare fields with mixed vegetation. In consequence, the spectral albedo characterization database for the other biomes was done using different strategy. For that, the United States Geological Survey (USGS) spectral library (USGSspeclib) (Kokaly et al., 2017) and the Ecosystem Spaceborne Thermal Radiometer Experiment on Space Station (ECOSTRESS) library (Meerdink et al., 2019) provides different reflectance signatures. These data represent a conical-conical reflectance obtained from different in-situ and airborne sources (Nicodemus et al., 1977; Schaepman-Strub et al., 2006). Although they do not represent either a directional-hemispherical or bi-hemispherical reflectances, they can be used as an approximation (Liang, 2001; Samain et al., 2006) when the surface is near-Lambertian (i.e., spectral albedo is equivalent to spectral reflectance) or the surface has no strong directionality and the spectral reflectance shape is not measured under critical areas such as hot-spot. The selection of reflectance curves in the database discarded those spectra that were not essentially representative of a Sentinel-3 pixel (e.g., rocks, mineral and meteorites), or spectral ranges not representative for Sentinel-3 configuration.

The synthetic dataset of downwelling irradiance was generated using the Second Simulation of a Satellite Signal in the Solar Spectrum, version 1 (6SV1) (Vermote et al., 1997). The simulation was performed from 300nm up to 2600nm in steps of 1nm (slightly below 6SV1 resolution). Above that spectral range up to 4000nm, it was set to zero to reduce computing time since the irradiance can be considered negligible. The parameterisation of 6SV1 was specific for each biome in terms of aerosol optical thickness (AOT), water vapour (WV), altitude and sun zenith angle. AOT and WV maps from March 2019 to March 2020 and an altitude map were obtained from NASA Earth

Observation (NEO, https://neo.gsfc.nasa.gov/) at a 0.1°spatial resolution. Viewing angles were set to nadir, ozone to 0.330 atm-cm, the atmosphere to mid-latitude summer and aerosol type to continental.

The spectral albedo and downwelling irradiance described above define both the simulated broadband albedo (a_γ) and simulated spectral albedos in Sentinel-3 bands (a_λ). The latter require the further convolution of the spectral albedo and downwelling irradiance by the mean spectral response functions of OLCI (S3 CalVal Team, 2016a, 2016b) and SLSTR (Nightingale, 2017, 2015). Then, a linear regression between them considering weights proportional to the land cover area in Table 7, defines the coefficients that represent a VIS/NIR/BB spectral region for both BSA and WSA albedos. The coefficients for Sentinel-3A and Sentinel-3B satellites (Table 8) include specific coefficients for the biome snow and for the rest of biomes (snow free, referred in the table as *glob*). Since the algorithm uses observations of both satellites, the mean value for each coefficient is used by the processing chain.

Table 8: Sentinel-3 albedo narrowband to broadband coefficients.

Satellite / Land cover coverage / Albedo type			$C_{0\gamma}$	$C_{\lambda\gamma}$								
			Interc.	Oa03	Oa04	Oa07	Oa17	Oa21	S1	S2	S5	S6
Sentinel-3 A	global	AL-DH-VI	0.0016	0.1732	0.2422	0.2755			0.1984	0.1048		
		AL-DH-NI	0.0007				0.5630	0.0833			0.2530	0.0856
		AL-DH-BB	-0.0010	-0.0746	0.2793	0.8184	0.0721	0.2975	-0.0909	-0.4972	0.1174	0.0294
		AL-BH-VI	0.0016	0.2808	0.2334	0.2079			0.1700	0.0828		
		AL-BH-NI	-0.0010				0.6620	0.0167			0.2425	0.0655
		AL-BH-BB	0.0002	-0.0127	0.238	0.6372	0.1221	0.2202	-0.0357	-0.3567	0.1028	0.0351
	snow	AL-DH-VI	-0.0002	0.2060	0.1478	0.0438			0.2918	0.3111		
		AL-DH-NI	0.0050				0.4469	0.2627			-0.0997	0.3323
		AL-DH-BB	-0.0010	-0.2862	0.6762	0.9336	0.2140	0.2121	-0.2979	-0.6213	0.0721	0.0943
		AL-BH-VI	-0.0004	0.3535	0.1462	-0.0284			0.2660	0.2633		
		AL-BH-NI	0.0059				0.5288	0.2298			-0.1798	0.3542
		AL-BH-BB	-0.0014	-0.3631	0.9954	0.8732	0.2305	0.1757	-0.3820	-0.6845	0.0199	0.1206
Sentinel-3 B	global	AL-DH-VI	0.0018	0.1630	0.2604	0.2871			0.1928	0.0908		
		AL-DH-NI	0.0007				0.5616	0.0851			0.2527	0.0856
		AL-DH-BB	-0.0010	-0.0697	0.2722	0.8215	0.0722	0.2977	-0.0955	-0.4935	0.1172	0.0293
		AL-BH-VI	0.0018	0.2721	0.2496	0.2290			0.1609	0.0631		
		AL-BH-NI	-0.0010				0.6605	0.0184			0.2427	0.0650
		AL-BH-BB	0.0002	-0.0105	0.2356	0.6439	0.1220	0.2207	-0.0411	-0.3579	0.1029	0.0348
	snow	AL-DH-VI	-0.0002	0.2093	0.1451	0.0460			0.2932	0.3068		
		AL-DH-NI	0.0049				0.4476	0.2614			-0.0985	0.3311
		AL-DH-BB	-0.0011	-0.3046	0.7006	0.9201	0.2113	0.2141	-0.3096	-0.6007	0.0800	0.0876
		AL-BH-VI	-0.0004	0.3569	0.1433	-0.0255			0.2668	0.2590		
		AL-BH-NI	0.0057				0.5295	0.2285			-0.1786	0.3527
		AL-BH-BB	-0.0014	-0.3907	1.0381	0.9135	0.2276	0.1784	-0.4260	-0.6949	0.0306	0.1115

The fitting error represents the difference between the simulated broadband albedo, the broadband albedo reconstructed using the coefficients in Table 8 and the Sentinel-3 band-convolved albedo. Table 9 summarizes the fitting results. It contains the level of correlation (R^2) and the weighted standard deviation of the errors (i.e. STD, considers the weight for each biome). The levels of correlation are high (R^2>0.99) and the residual error is low (std<0.01) for all cases. These values are in line with fitting results that can be found for other studies and missions (Liang, 2001; Van Leeuwen and Roujean, 2002).

Table 9: Fitting error (STD) and correlation (R^2) of C3S Sentinel-3 narrowband to broadband albedo coefficients presented in Table 8

Land cover	Param.	AL-DH-VI	AL-DH-NI	AL-DH-BB	AL-BH-VI	AL-BH-NI	AL-BH-BB
global	R^2	0.9997	0.9962	0.9905	0.9975	0.9939	0.9961
global	STD	0.0012	0.0049	0.0051	0.0038	0.0061	0.0030
snow	R^2	1.0000	0.9996	0.9996	1.0000	0.9993	1.0000
snow	STD	0.0001	0.0056	0.0058	0.0007	0.0074	0.0018

4.1.5. Uncertainty propagation

The C3S SA products include an uncertainty estimate associated to the different broadband albedo values. This uncertainty is the result of propagation through the retrieval chain, taking as starting point the uncertainty of the BRDF retrieval module. This is explained as the Sentinel-3 input does not currently include uncertainty information. Then, we start from approximated (synthetic) uncertainties in the BRDF retrieval step (Leon-Tavares, 2020).

As BRDF model parameters and spectral albedos have a linear relationship, the error covariance matrix of the model parameters is used for standard ("1-sigma") error estimates of the spectral albedo quantities (Lucht and Lewis, 2000). Then, the uncertainty of the spectral albedos is estimated by propagating the BRDF retrievals variances through the spectral albedos polynomial computations. On the other hand, assuming that the errors of the narrow to broadband linear relationship are uncorrelated by the dependence of the spectral wavelength, the broadband albedo quantity error estimates can be expressed by the following expression:

$$\sigma[a_\gamma] = \sqrt{\sum_\lambda \left(\frac{\sigma_{a\lambda}{}^2}{a_\lambda{}^2} + \frac{\sigma_{\lambda\gamma}{}^2}{c_{\lambda\gamma}{}^2} \right) * \left(c_{\lambda\gamma} a_\lambda \right)^2} \qquad \text{Eq. 4}$$

where $\sigma_{\lambda\gamma}$ are the errors of the spectral integration coefficients, and the fitting error of these coefficients (see STD parameter in Table 9) are used as an approximation for the uncertainty (Liang, 2001).

4.1.6. Output products

The output of the processing consists in 4 sets of products, for either directional-hemispherical reflectances (variables named DH) or bi-hemispherical reflectances (BH), and for the spectral albedos (ALSP) or the broadband albedos (ALBB), all distributed as separate files. Products are globally displayed on Plate Carrée regular latitude/longitude projection (with the ellipsoid WGS 1984), as detailed in the coordinates reference system variable metadata. The resolution of the grid is 1/3360, giving respectively aproximately 300 m of pixel extent at the equator. The files of version 3.0 of Surface Albedo products are generated in Network Common Data Form version 4 (NetCDF4) format, internally compressed. Metadata attributes are compliant with climate and forecast conventions.

The ALSP-DH and ALSP-BH products contain the spectral albedos and their corresponding uncertainties and quality flags (QFLAG), for each OLCI (Oa03, Oa04, Oa07, Oa17, Oa21) and SLSTR (S1, S2, S5, S6) channel. The ALBB-DH and ALBB-BH products contain the broadband albedos and their corresponding uncertainties and QFLAG, available for the three spectral domains (VI, NI, BB). More information about the product can be found in the product documentation (Sánchez-Zapero et al., 2021a).

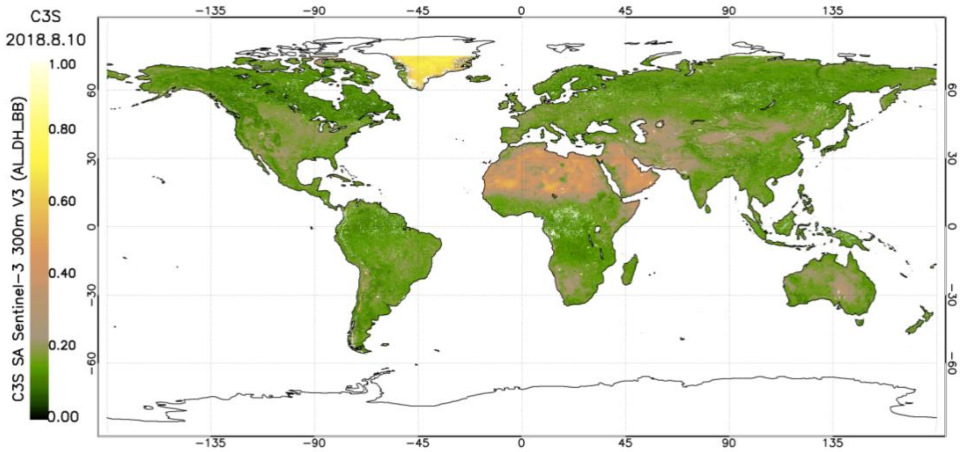

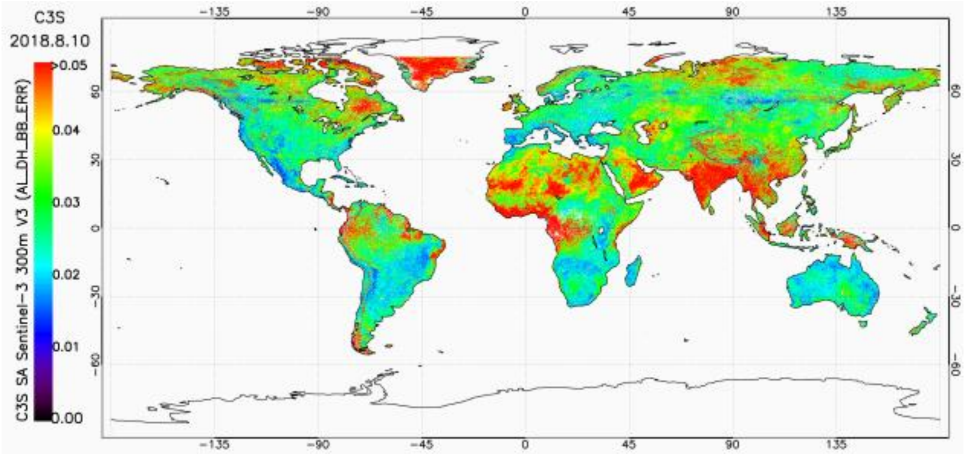

Figure 3: Global maps of C3S Sentinel-3 SA v3.0 AL-DH-BB (top) for 10th August 2018 and associated uncertainty (bottom).

5. Quality assessment results

5.1. Temporal consistency

Sentinel-3 SA v3.0 temporal variations are analysed over the globally representative LANDVAL network of sites for each main land cover, and qualitatively compared with the other satellite references (C3S PROBA-V SA v1.0, MCD43A3 C6).

-C3S Sentinel-3 V3 -C3S PROBA-V V1 -MCD43A3 C6 ● SNOW xNo data in dekad

Figure 4 illustrates the typical temporal trend of the albedo products for each main biome type.

Note that Sentinel-3 SA v3.0 quality flag information is displayed in the temporal profiles: dots represent pixels identified with 'probability' of snow, and crosses represent retrievals where no data is available during the composite period. Vertical bars of Sentinel-3 SA v3.0 correspond to associated error auxiliary layer. MCD43A3 C6 pixels classified as snow according to quality product dataset (MCD43A2) are also identified with dots.

For Evergreen Broadleaved Forest (EBF), typically located over equatorial areas, Sentinel-3 SA v3.0 shows remarkable stable temporal trajectories and noteworthy good completeness. The other satellite products (C3S SA v1.0, MCD43A3 C6) display larger number of missing values and nosier profiles. For the other forest cases, such as Needle-Leaf (NLF, which is mainly distributed at northern latitudes) and Deciduous Broadleaved (DBF) Forests, Sentinel-3 SA v3.0 fit temporally well with reference satellite products, properly reproducing the typical situations over these cases: periods with stable values, slight changes due to seasonality and rapid and large changes in magnitude due to snow events. Note that Sentinel-3 SA v3.0 algorithm tends to identify lower number of snow cases than MCD43A3 C6 during the common periods (see for instance December 2018 – April 2019 in LANDVAL#233), but it can deal with this issue providing reliable snow albedo values and improving the completeness due to persistent cloud coverage. For long periods with low availability of data in the transitions from snow-free to snow coverage (e.g., November-December 2018 in LANDVAL#564), Sentinel-3 tends to provide slower transition from low to high albedo values than the expected trend (rapid albedo changes). This can be explained by the low availability of input data. If observations are not available, the model cannot react immediately.

Close temporal patterns are noticed between sensors over cultivated areas and other biomes (herbaceous or shrublands), well reproducing the phenology of the crops or variations due to natural vegetation. In case of bare areas targets, C3S Sentinel-3 SA v3.0 properly provides stable temporal trends.

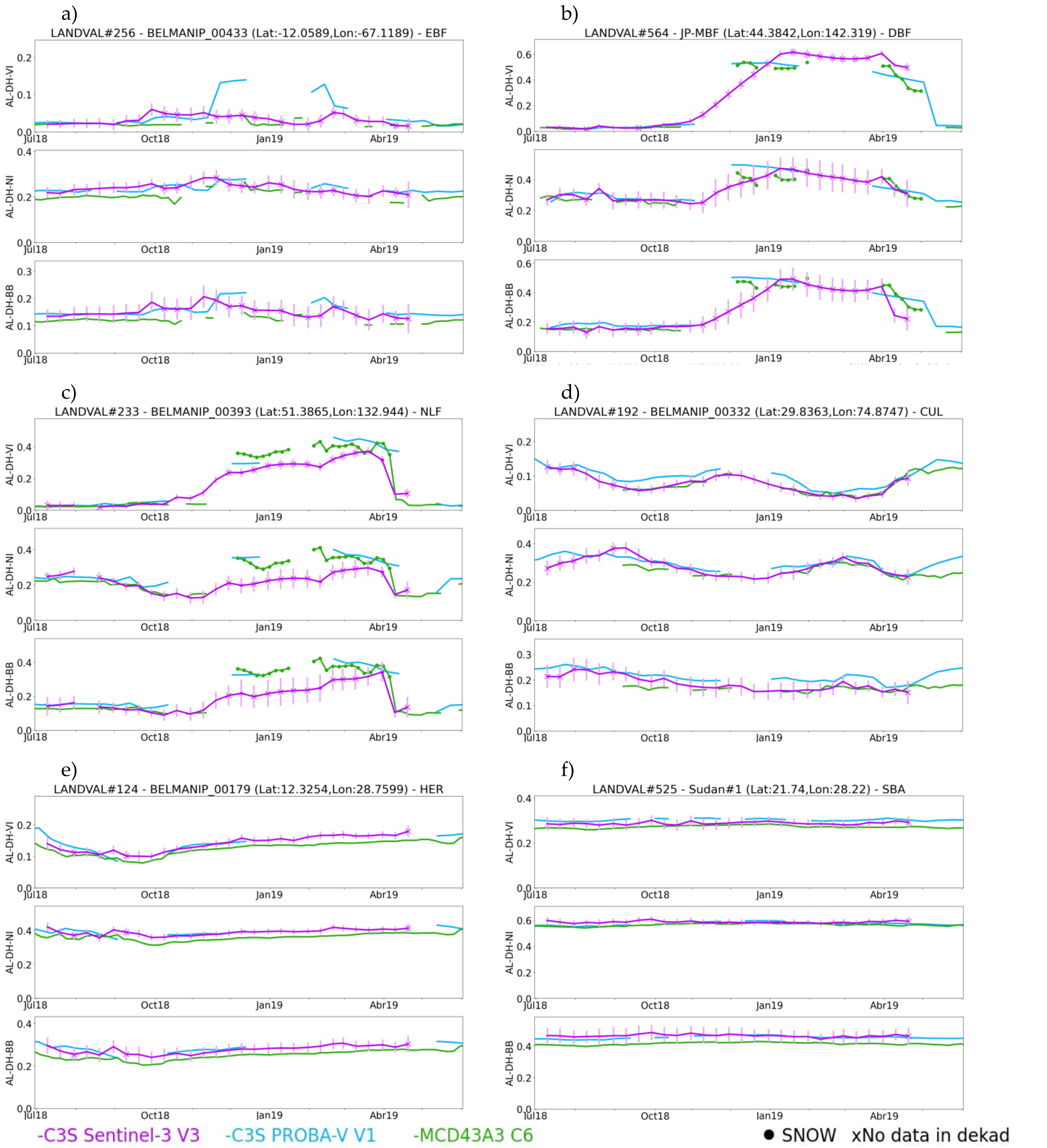

Figure 4: Temporal profiles of C3S Sentinel-3 SA v3.0 (purple), C3S PROBA-V SA v1.0 (blue) and MCD43A3 C6 (green) for July2018-June2019 period. Examples over one selected LANDVAL site representing the main biome types (a) EBF, b) DBF, c) NLF, d) CUL, e) HER, f) SBA). For Sentinel-3 SA v3.0, dots and crosses represent pixels identified with 'probability of snow' and 'no data available during the dekad', respectively. In case of MCD43A3 C6, dots represent pixels classified as snow.

5.2. Error evaluation (product intercomparison)

The overall error between C3S Sentinel-3 SA v3.0 was evaluated through product intercomparison with satellite references (C3S PROBA-V SA v1.0, MCD43A3 C6). LANDVAL network of sites was used for sampling global conditions, and the period of the study corresponds to the availability of Sentinel-3 demonstration dataset (July 2018-April 2019).

5.2.1. Overall consistency between C3S Sentinel-3 SA v3.0 vs C3S PROBA-V v1.0

Scatter-plots of total shortwave BSA with associated metrics are displayed in Figure 5, as well as the box-plots of the diffference per range albedo value (bottom). The performance figures for both BSA and WSA are summarized in Table 10 for the three broadband ranges.

Good correlations were found for visible domain (R=0.92) with almost no bias for black-sky albedos (MD~0) and negative MD of -4.2% for white-sky albedo. Box-plots show the slight median negative bias (Sentinel-3 < PROBA-V) for almost all SA ranges, except for the higher values (from 0.8 to 1, positive bias). In overall, negative bias (MD) (Sentinel-3 < PROBA-V) of around -5% was found for NIR, with RMSD of around 0.05 (~15%). Similarly, Sentinel-3 SA v3.0 have a tendency to display lower retrievals than PROBA-V SA v1.0 (MD of -5.7% for AL-DH-BB, and -8.4% for AL-BH-BB) for the total shortwave, with overall uncertainties (RMSD) of around 0.05 (~ 20%). The negative bias was found for most of the product ranges (with the exception of albedo values higher than 0.6 in NIR and 0.8 in total shortwave). Typically around 20% - 40% of cases are within the optimal (GCOS) uncertainty requirements, and typically around 50% considering the target level (C3S KPI).

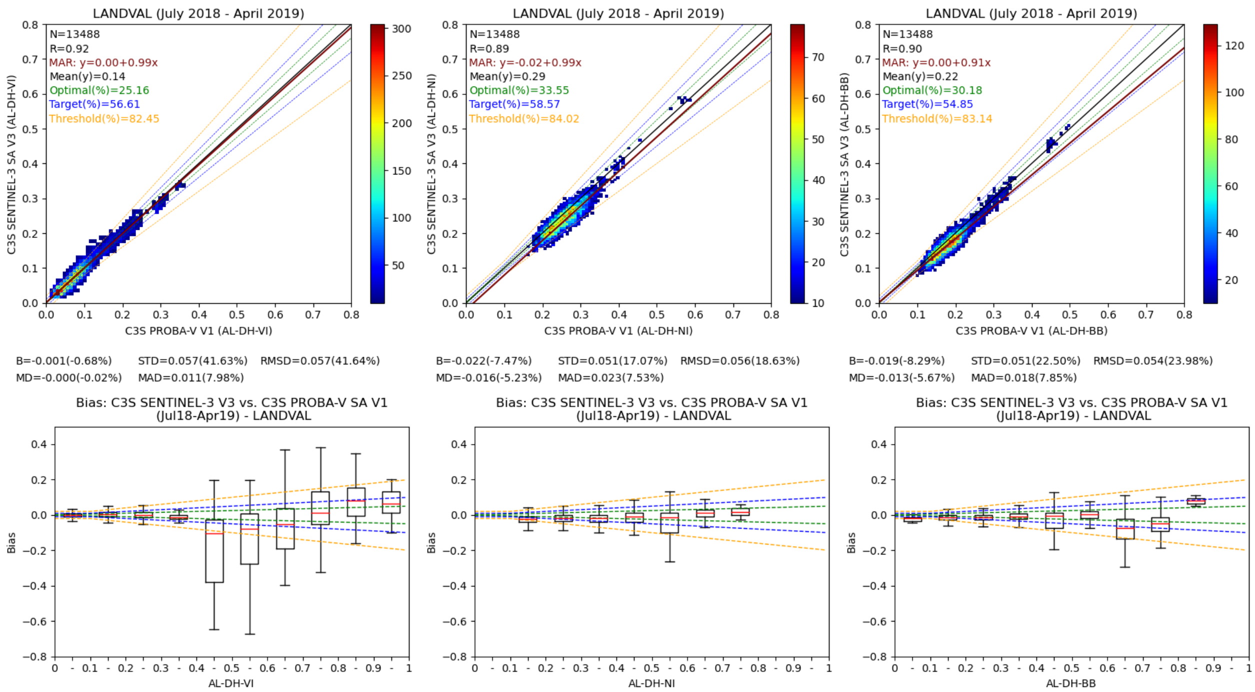

Figure 5: Top: Scatter-plots (AL-DH-VI, AL-DH-NI, AL-DH-BB) between C3S Sentinel-3 SA v3.0 (average of 3x3 pixels) (Y-axis) versus C3S PROBA-V SA v1.0 (one high quality pixel) (X-axis) products from July 2018 to April 2019. Green, blue and orange dashed lines correspond to optimal, target and threshold predefined levels around continuous black 1:1 line. MAR is represented in Red line. Bottom: Box-plots bias per range albedo value. Red bars of boxes display median values, boxes stretch from the 25th to the 75th percentiles of the data and whiskers include 99.3% of the coverage data (±2.7 σ). Outliers are not displayed.

Table 10: Performance statistics between C3S Sentinel-3 SA v3.0 versus C3S PROBA-V SA v1.0 products. Computation in July 2018 to April 2019 over LANDVAL.

	C3S Sentinel-3 SA v3.0 versus C3S PROBA-V SA v1.0					
	AL-DH-VI	AL-DH-NI	AL-DH-BB	AL-BH-VI	AL-BH-NI	AL-BH-BB
Correlation	0.92	0.89	0.90	0.92	0.92	0.92
Bias (%)	-0.001 (-0.7%)	-0.022 (-7.5%)	-0.019 (-8.3%)	-0.008 (-5.6%)	-0.013 (-4.0%)	-0.023 (-9.8%)
MD (%)	<-0.001 (0.0%)	-0.016 (-5.2%)	-0.013 (-5.7%)	-0.006 (-4.2%)	-0.009 (-2.8%)	-0.020 (-8.4%)
STD (%)	0.057 (41.6%)	0.051 (17.1%)	0.051 (22.5%)	0.056 (40.7%)	0.044 (13.8%)	0.044 (18.5%)
MAD (%)	0.011 (8.0%)	0.023 (7.5%)	0.018 (7.9%)	0.014 (10.2%)	0.021 (6.7%)	0.023 (9.6%)
RMSD (%)	0.057 (41.6%)	0.056 (18.6%)	0.054 (24.0%)	0.056 (41.1%)	0.046 (14.4%)	0.049 (20.9%)
MAR	y=0.00+0.99x	y=-0.02+0.99x	y=0.00+0.91x	y=0.00+0.97x	y=-0.02+1.01x	y=-0.01+0.95x
%optimal (GCOS)	25.2	33.6	30.2	18.3	37.7	24.0
%target (C3S KPI)	56.6	58.6	55.9	45.5	63.1	48.0

5.2.2. Overall consistency between C3S Sentinel-3 SA v3.0 vs MCD43A3 C6

This section shows the overall comparison of C3S Sentinel-3 SA v3.0 vs MCD43A3 C6. Scatter-plots and analysis of bias per range albedo BSA total shortwave albedo value are displayed in Figure 6. The summary of all performance statistics for both BSA and WSA in all broadband ranges (visible, NIR and total shortwave) is presented in Table 11.

Mean negative bias of -1.8% (-5.2%) is observed for visible domain (AL-DH-VI, AL-BH-VI) with positive median value (MD) of 6% (1.6%). Differences in the sign of the bias between mean and median values are due to outliers over snow cases (Sentinel-3 < MCD43A3 C6), and median values are more realistic to report the accuracy in those cases. These outliers are due to underestimation of snow albedo values in case of Sentinel-3 and to the slow transition between snow-free and snow-covered seasons, as observed in the temporal consistency analysis. For the near infrared, the accuracy of Sentinel-3 SA v3.0 compared with MCD43A3 C6 showed, in overall, positive sign with MD of 4.2% and 7.2% for BSA and WSA. For the total shortwave, in overall, positive MD of 6-7% was found. Box-plots clearly display the slight median positive bias (Sentinel-3 > MCD43A3 C6) for the lower albedo values (where most of pixels are located) and large negative for highest albedos (typically snow cases). Regardless the uncertainty requirements, typically between 20% and 30% of cases achieved optimal (GCOS) level of consistency, and more than 50% of cases within target level (C3S KPI).

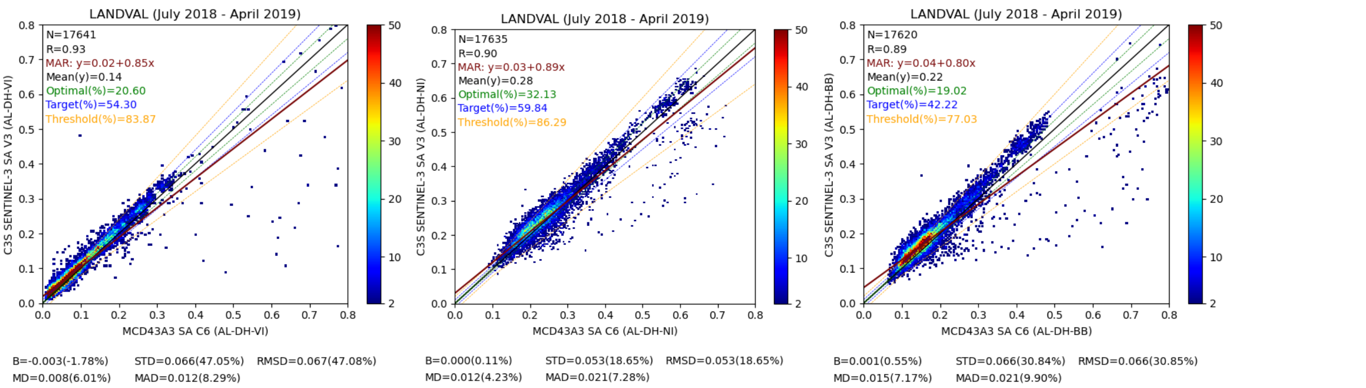

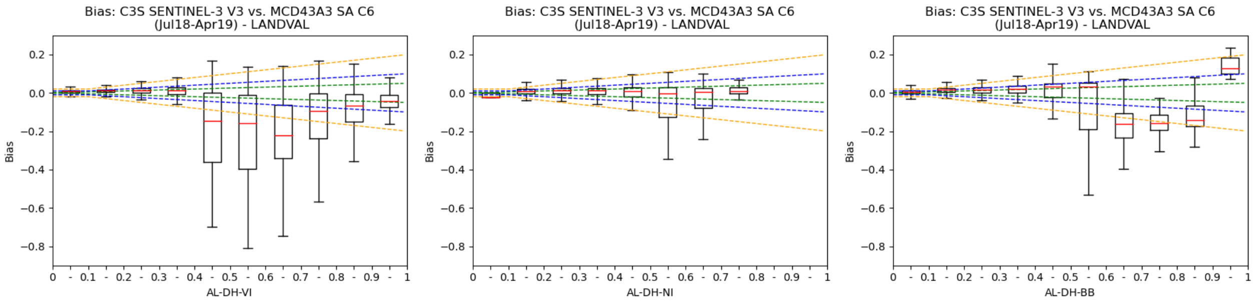

Figure 6: Top: Scatter-plots (AL-DH-VI, AL-DH-NI, AL-DH-BB) between C3S Sentinel-3 SA v3.0 (average of 3x3 pixels) (Y-axis) versus MCD43A3 C6 (average of 2x2 good quality pixels) (X-axis) products from July 2018 to April 2019. Green, blue and orange dashed lines correspond to optimal, target and threshold predefined levels around continuous black 1:1 line. MAR is represented in Red line. Bottom: Box-plots of bias per range albedo value. Red bars of boxes display median values, boxes stretch from the 25th to the 75th percentiles of the data and whiskers include 99.3% of the coverage data (±2.7 σ). Outliers are not displayed.

Table 11: Performance statistics between C3S Sentinel-3 SA v3.0 versus MCD43A3 C6 products. Computation in July 2018 to April 2019 over LANDVAL sites.

	C3S Sentinel-3 SA v3.0 versus MCD43A3 SA C6					
	AL-DH-VI	AL-DH-NI	AL-DH-BB	AL-BH-VI	AL-BH-NI	AL-BH-BB
Correlation	0.93	0.90	0.89	0.94	0.93	0.92
Bias (%)	-0.003 (-1.8%)	<0.001 (0.1%)	0.001 (0.6%)	-0.007 (-5.2%)	0.017 (5.7%)	0.003 (1.3%)
MD (%)	0.008 (6.0%)	0.012 (4.2%)	0.015 (7.2%)	0.002 (1.6%)	0.022 (7.2%)	0.013 (5.7%)
STD (%)	0.066 (47.1%)	0.053 (18.7%)	0.066 (30.8%)	0.063 (44.8%)	0.043 (14.4%)	0.056 (25.2%)
MAD (%)	0.012 (8.3%)	0.021 (7.3%)	0.021 (9.9%)	0.009 (6.1%)	0.026 (8.5%)	0.017 (7.6%)
RMSD (%)	0.067 (47.1%)	0.053 (18.7%)	0.066 (30.9%)	0.064 45.1%)	0.046 (15.4%)	0.056 (25.3%)
MAR	y=0.02+0.85x	y=0.03+0.89x	y=0.04+0.80x	y=0.01+0.85x	y=0.04+0.92x	y=0.04+0.83x
%optimal (GCOS)	20.6	32.1	19.0	31.6	27.1	28.2
%target (C3S KPI)	54.3	59.8	42.2	66.2	53.2	55.7

5.2.3. Analysis per biome type

The Probability density function distributions of Sentinel-3 SA v3.0 (Figure 7) albedo retrievals per main biome type are evaluated and qualitatively compared with reference products (MCD43A3 C6, C3S PROBA-V SA v1.0).

C3S Sentinel-3 SA v3.0 products showed similar distribution of retrievals than both satellite references for most biome types in all spectral broadband ranges, except over EBF biome type, where both C3S products tend show values toward higher values compared with MCD43A3 C6. Note that EBF biome type is typically mainly affected by cloud contamination. Both C3S products also tend to provide slight tendency to high albedo values than MCD43A3 C6 for DBF, NLF, cultivated and herbaceous for the total shortwave.

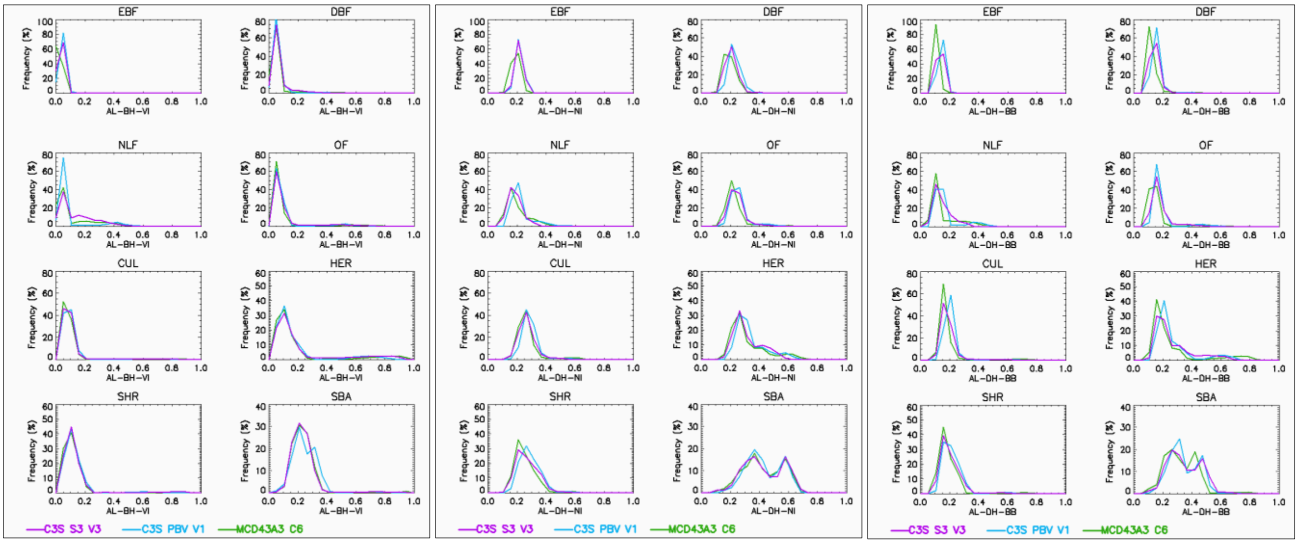

Figure 7: Distribution of black-sky broadband albedo values for visible (left), NIR (center) and total shortwave (right) per main biome type. Comparison between C3S Sentinel-3 SA v3.0 (purple), C3S PROBA-V SA v1.0 (blue) and MCD43A3 C6 (green) products at 1km² resolution in July 2018 to April 2019 period over LANDVAL sites.

5.3. Error evaluation (direct validation)

Figure 8 shows the scatter-plots of the validation of satellite datasets (C3S Sentinel-3 SA v3.0 and PROBA-V SA v1.0, and MCD43A3 C6) compared with measurements from 33 ground stations. The validation metrics are summarized in Table 12. The footprint of ground measurement is homogeneous at 1 km² area (see Annex II), and the comparison was performed using the primary resolution of PROBA-V based products, and average of 3x3 and 2x2 windows in case of Sentinel-3 and MODIS based products.

Sentinel-3 SA v3.0 provides slightly worse accuracy than MCD43A3 C6, and opposite sign of differences: MD=6.3% in case of Sentinel-3 SA v3.0, and MD=-3.3% in case of MCD43A3 C6. PROBA-V SA v1.0 provides larger positive systematic differences (MD=15.8%), in line to that found in previous exercises (Sánchez-Zapero et al., 2020).

The three satellite products provided similar results in terms of precision (STD, MAD) and overall uncertainty (RMSD). MCD43A3 C6 provided the best precision (MAD=8.6%) and uncertainty (RMSD=22.1%). Worse agreement was found for PROBA-V SA v1.0 (MAD=18.1%, RMSD=25.6%), whereas intermediate results were found for Sentinel-3 SA v3.0 (MAD=13.9%, RMSD=24.2%).

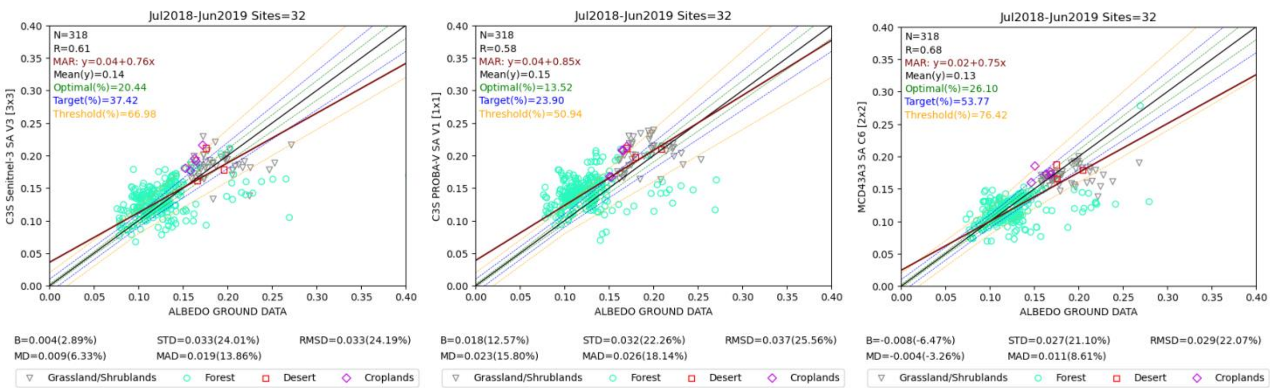

Figure 8: Direct validation of satellite albedo products (from left to right: C3S Sentinel-3 SA v3.0, C3S PROBA-V SA v1.0, MCD43A3 C6) versus ground values from July 2018 to April 2019 at 1 km^2 of spatial resolution. Green, blue and orange dashed lines correspond to optimal (GCOS), target (C3S KP) and threshold predefined uncertainty levels around continuous black 1:1 line. MAR is represented in Red line.

Table 12: Direct validation relevant statistics of satellite albedo products (C3S Sentinel-3 SA v3.0, C3S PROBA-V SA v1.0 and MCD43A3 C6) products versus albedo ground values at 1 km^2 of spatial resolution during the July 2018-April 2019 period.

	C3S S-3 SA v3.0	C3S PBV SA v1.0	MCD43A3 C6
Stations (N)	32 (318)		
Correlation	0.61	0.58	0.68
Bias	0.004 (2.9%)	0.018 (12.6%)	-0.008 (-6.5%)
MD	0.009 (6.3%)	0.023 (15.8%)	-0.004 (-3.3%)
STD	0.033 (24.0%)	0.032 (22.3%)	0.027 (21.1%)
MAD	0.019 (13.9%)	0.026 (18.1%)	0.011 (8.6%)
RMSD	0.033 (24.2%)	0.037 (25.6%)	0.029 (22.1%)
Offset (MAR)	0.04	0.04	0.02
Slope (MAR)	0.76	0.85	0.75
%optimal (GCOS)	20.4	13.5	26.1
%target (C3S KPI)	37.4	23.9	53.8

6. Summary and conclusions

The Climate Change Service of Copernicus undertook an initiative with aim to provide operational global estimates of the surface albedo based on Sentinel-3 OLCI and SLSTR observations, which is implemented in the C3S Sentinel-3 SA v3.0 prototype. The SA C3S existing CDR continuity is ensured thanks to the switch to Surface Albedo v3.0 algorithm. In the past, C3S CDR is based on NOAA/AVHRR (September 1981-2005), SPOT/VGT (April 1998 - May 2014) and PROBA-V (November 2013 – June 2020). C3S Sentinel-3 also provides improved spatial resolution (300 m versus 1 km and 4 km for Vegetation and AHVRR sensors) and richer spectral information (nine spectral albedos versus four) compared to previous datasets. The SA v3.0 responds to the GCOS requirement for an improved spatial resolution (200/500 m) of satellite-based EO products.

The quality assessment is performed over a limited demonstration test dataset covering 10 months (from July 2018 to April 2019). The validation is performed considering global conditions, expanding the spatial and temporal coverage of the quality assessment of initial developments of the prototype (Sanchez-Zapero et al., 2021). This preliminary scientific evaluation demonstrated that C3S Sentinel-3 SA v3.0 pre-operational product is good enough to guarantee continuation of PROBA-V time series, as it shows good overall consistency with other products and similar performance against in-situ observations. Time and space good agreements are noticed between C3S Sentinel-3 SA v3.0 and reference satellite datasets (C3S PROBA-V SA v1.0, MCD43A3 C6), with overall discrepancies (RMSD) of around 0.05. The comparison with ground data shows similar accuracy than MCD43A3 C6 but opposite sign of differences (slight positive in case of Sentinel-3), improving the accuracy of C3S products based on PROBA-V.

The main drawback is the underestimation of snow albedo values, due to the current limitation related to input data from the ESA Sentinel-3 mission. In particular IdePix processor, used in the CGLS pre-processing chain does not provide a correct identification of snow pixels. For that, Surface Albedo v3.0 algorithm incorporated and alternative decision rule in the prototype based on NDSI index, that was able to identify large quantity of snow cases, but providing underestimation of snow albedo values (-20% compared to MCD43A3 C6). The consequence is the low quantity of good quality observations (based on IdePix) ingested as input data in the BRDF retrieval. The algorithm can deal with low availability of input data due to the use of BRDF prior information based on MODIS BRDF climatology.

Additionally, vicarious TOA SLSTR calibration coefficients (S3_MPC, 2021b) were not used in the CGLS pre-processing chain to correct the systematic negative bias (mainly observed in S5 and S6 channels). We applied these calibration coefficients directly to spectral albedos, and corrected the bias compared with MCD43A3 C6 in more than 10 points in relative terms.

The shortcomings of the product (cloud/snow identification and calibration coefficients) can be overcome with future improved input data, which would justify the reprocessing of a new version.

The data can be accessed through the CDS using this link: https://cds.climate.copernicus.eu/cdsapp#!/dataset/satellite-albedo?tab=overview.

Acknowledgements

This work was developed in the framework of the Copernicus Climate Change Service (COP_059 contract). The Sentinel-3 Surface Albedo v3.0 algorithm was developed by EOLAB and the product is a data set produced by VITO. The product is based on Sentinel-3 TOC reflectances, which are provided by Copernicus Global Land Service.

References

Amut, A., Gong, L., Yuan, Z., 2007. Spatial distributions of surface albedo from satellite data in arid oasis. https://doi.org/10.1117/12.746119 6679, 550–555. https://doi.org/10.1117/12.746119

Baret, F., Weiss, M., Lacaze, R., Camacho, F., Makhmara, H., Pacholcyzk, P., Smets, B., 2013. GEOV1: LAI and FAPAR essential climate variables and FCOVER global time series capitalizing over existing products. Part1: Principles of development and production. Remote Sens. Environ. 137, 299–309. https://doi.org/10.1016/j.rse.2012.12.027

Barnsley, M.J., Strahler, A.H., Morris, K.P., Muller, J.P., 1994. Sampling the surface bidirectional reflectance distribution function (BRDF): 1. evaluation of current and future satellite sensors. Remote Sens. Rev. 8, 271–311. https://doi.org/10.1080/02757259409532205

Bartholome, E., Belward, A., 2005. GLC2000: a new approach to global land cover mapping from Earth observation data. Int. J. Remote Sens. 26, 1959–1977. https://doi.org/10.1080/01431160412331291297

Betts, A.K., 2009. Land-Surface-Atmosphere Coupling in Observations and Models. J. Adv. Model. Earth Syst. 1, n/a-n/a. https://doi.org/10.3894/JAMES.2009.1.4

Breon, F.-M., Maignan, F., 2017. A BRDF–BPDF database for the analysis of Earth target reflectances. Earth Syst. Sci. Data 9, 31–45. https://doi.org/10.5194/essd-9-31-2017

Bréon, F.-M., Vermote, E., 2012. Correction of MODIS surface reflectance time series for BRDF effects. Remote Sens. Environ. 125, 1–9. https://doi.org/10.1016/j.rse.2012.06.025

Carrer, D., Ceamanos, X., Pinault, F., Benhadj, I., Toté, C., 2019. Algorithm Theoretical Basis Document (ATBD) of PROBA-V CDR and ICDR Surface Albedo v1.0 (Official reference number service contract: 2018/C3S_312b_Lot5_VITO/SC1). [WWW Document]. Tech. Rep. Prep. Copernicus Clim. Chang. Serv. URL https://datastore.copernicus-climate.eu/documents/satellite-albedo/D1.3.3-v1.0_ATBD_CDR-ICDR_SA_PROBAV_v1.0_PRODUCTS_v1.0.2.pdf (accessed 5.2.22).

Carrer, D., Pinault, F., Lellouch, G., Trigo, I.F., Benhadj, I., Camacho, F., Ceamanos, X., Moparthy, S., Munoz-Sabater, J., Schüller, L., Sánchez-Zapero, J., 2021. Surface Albedo Retrieval from 40-Years of Earth Observations through the EUMETSAT/LSA SAF and EU/C3S Programmes: The Versatile Algorithm of PYALUS. Remote Sens. 13, 372. https://doi.org/10.3390/rs13030372

Carrer, D., Roujean, J.L., Meurey, C., 2010. Comparing operational MSG/SEVIRI Land Surface albedo products from Land SAF with ground measurements and MODIS. IEEE Trans. Geosci. Remote Sens. 48, 1714–1728. https://doi.org/10.1109/TGRS.2009.2034530

Cescatti, A., Marcolla, B., Santhana Vannan, S.K., Pan, J.Y., Román, M.O., Yang, X., Ciais, P., Cook, R.B., Law, B.E., Matteucci, G., Migliavacca, M., Moors, E., Richardson, A.D., Seufert, G., Schaaf, C.B., 2012. Intercomparison of MODIS albedo retrievals and in situ measurements across the global FLUXNET network. Remote Sens. Environ. 121, 323–334. https://doi.org/10.1016/j.rse.2012.02.019

Claverie, M., Vermote, E., Franch, B., He, T., Hagolle, O., Kadiri, M., Masek, J., 2015. Evaluation of Medium Spatial Resolution BRDF-Adjustment Techniques Using Multi-Angular SPOT4 (Take5) Acquisitions. Remote Sens. 7, 12057–12075. https://doi.org/10.3390/rs70912057

Dickinson, R.E., 1995. Land processes in climate models. Remote Sens. Environ. 51, 27–38. https://doi.org/10.1016/0034-4257(94)00062-R

Diner, D.J., Beckert, J.C., Reilly, T.H., Bruegge, C.J., Conel, J.E., Kahn, R.A., Martonchik, J. V., Ackerman, T.P., Davies, R., Gerstl, S.A.W., Gordon, H.R., Muller, J.P., Myneni, R.B., Sellers, P.J., Pinty, B., Verstraete, M.M., 1998. Multi-angle imaging spectroradiometer (MISR) instrument description and experiment overview. IEEE Trans. Geosci. Remote Sens. 36, 1072–1087. https://doi.org/10.1109/36.700992

Diner, D.J., Martonchik, J. V, Borel, C., Gerstl, S.A.W., Gordon, H.R., Knyazikhin, Y., Myneni, R., Pinty, B., Verstraete, M.M., 2008. Level 2 Surface Retrieval Algorithm Theoretical Basis Level 2 Surface Retrieval Algorithm Theoretical Basis Approval.

Doxani, G., Vermote, E., Roger, J.-C., Gascon, F., Adriaensen, S., Frantz, D., Hagolle, O., Hollstein, A., Kirches, G., Li, F., Louis, J., Mangin, A., Pahlevan, N., Pflug, B., Vanhellemont, Q., 2018. Atmospheric Correction Inter-

Comparison Exercise. Remote Sens. 10, 352. https://doi.org/10.3390/rs10020352

Franch, B., Vermote, E.F., Sobrino, J.A., Julien, Y., 2014. Retrieval of Surface Albedo on a Daily Basis: Application to MODIS Data. IEEE Trans. Geosci. Remote Sens. 52. https://doi.org/10.1109/TGRS.2014.2313842

Fuster, B., Sánchez-Zapero, J., Camacho, F., García-Santos, V., Verger, A., Lacaze, R., Weiss, M., Baret, F., Smets, B., 2020. Quality Assessment of PROBA-V LAI, fAPAR and fCOVER Collection 300 m Products of Copernicus Global Land Service. Remote Sens. 12, 1017. https://doi.org/10.3390/rs12061017

GCOS-154, 2011. Systematic observation requirements for satellite-based data products for climate. Supplemental details to the satellite-based component of the "Implementation Plan for the GCOS in Support of the UNFCCC" [WWW Document]. URL https://library.wmo.int/doc_num.php?explnum_id=3710 (accessed 4.10.22).

GCOS-200, 2016. Space Agency Response to GCOS Implementation Plan [WWW Document]. URL https://gcos.wmo.int/en/gcos-implementation-plan (accessed 5.2.22).

Geiger, B., Carrer, D., Franchistéguy, L., Roujean, J.L., Meurey, C., 2008. Land surface albedo derived on a daily basis from meteosat second generation observations. IEEE Trans. Geosci. Remote Sens. 46, 3841–3856. https://doi.org/10.1109/TGRS.2008.2001798

Govaerts, Y.M., Lattanzio, A., Taberner, M., Pinty, B., 2008. Generating global surface albedo products from multiple geostationary satellites. Remote Sens. Environ. 112, 2804–2816. https://doi.org/10.1016/j.rse.2008.01.012

Gueymard, C.A., Lara-Fanego, V., Sengupta, M., Xie, Y., 2019. Surface albedo and reflectance: Review of definitions, angular and spectral effects, and intercomparison of major data sources in support of advanced solar irradiance modeling over the Americas. Sol. Energy. https://doi.org/10.1016/j.solener.2019.02.040

Harper, W. V., 2014. Reduced Major Axis regression: teaching alternatives to Least Squares. Proc. Ninth Int. Conf. Teach. Stat. 1–4. https://doi.org/10.1016/B978-0-12-420228-3.00013-0

Henderson-Sellers, A., Wilson, M.F., 1983. Surface albedo data for climatic modeling. Rev. Geophys. 21, 1743–1778. https://doi.org/10.1029/RG021I008P01743

Hu, B., Lucht, W., Li, X., Strahler, A.H., 1997. Validation of kernel-driven semiempirical models for the surface bidirectional reflectance distribution function of land surfaces. Remote Sens. Environ. 62, 201–214. https://doi.org/10.1016/S0034-4257(97)00082-5

Jacquemoud, S., Baret, F., 1990. PROSPECT: A model of leaf optical properties spectra. Remote Sens. Environ. 34, 75–91. https://doi.org/10.1016/0034-4257(90)90100-Z

Jacquemoud, S., Verhoef, W., Baret, F., Bacour, C., Zarco-Tejada, P.J., Asner, G.P., François, C., Ustin, S.L., 2009. PROSPECT + SAIL models: A review of use for vegetation characterization, Remote Sensing of Environment. Elsevier Inc. https://doi.org/10.1016/j.rse.2008.01.026

JCGM-GUM, 2008. Joint Committee for Guides in Metrology (JCGM) - Guides to the expression of Uncertainty in Measurement (GUM). [ISO/IEC Guide 98 - Part 3, 2008]. [WWW Document]. URL https://www.iso.org/sites/JCGM/GUM-introduction.htm (accessed 4.10.20).

Jolivet, D., 2021. "CGLOPS-1" Framework Service Contract N° 199494 (JRC). Quality Assessment Report of Atmospheric Correction for Sentinel-3 OLCI and SLSTR products [WWW Document]. URL https://land.copernicus.eu/global/sites/cgls.vito.be/files/products/CGLOPS1_QAR_S3-AC_I1.10.pdf (accessed 5.2.22).

Justice, C., Belward, A., Morisette, J., Lewis, P., Privette, J., Baret, F., 2000. Developments in the'validation'of satellite sensor products for the study of the land surface. Int. J. Remote Sens. 21, 3383–3390.

Kokaly, R.F., Clark, R.N., Swayze, G.A., Livo, K.E., Hoefen, T.M., Pearson, N.C., Wise, R.A., Benzel, W.M., Lowers, H.A., Driscoll, R.L., Klein, A.J., 2017. USGS Spectral Library Version 7, Data Series. https://doi.org/10.3133/DS1035

Lacherade, S., Fougnie, B., Henry, P., Gamet, P., 2013. Cross calibration over desert sites: Description, methodology, and operational implementation. IEEE Trans. Geosci. Remote Sens. 51, 1098–1113. https://doi.org/10.1109/TGRS.2012.2227061

Lellouch, G., Carrer, D., Vincent, C., Pardé, M., C. Frietas, S., Trigo, I.F., 2020. Evaluation of Two Global Land Surface Albedo Datasets Distributed by the Copernicus Climate Change Service and the EUMETSAT LSA-SAF. Remote Sens. 12, 1888. https://doi.org/10.3390/rs12111888

Leon-Tavares, J., 2020. Copernicus Global Land Operations "Vegetation and Energy". "CGLOPS-1" Framework Service Contract N° 199494 (JRC) Algorithm Theoretical Basis Document BRDF Model retrieval from Sentinel-3 Collection 300 m Version 1. Issue I1.00 [WWW Document]. URL https://land.copernicus.eu/global/sites/cgls.vito.be/files/products/CGLOPS1_ATBD_BRDFCorrection300m-V1_I1.00.pdf (accessed 5.2.22).

Leroy, M., Deuzé, J.L., Bréon, F.M., Hautecoeur, O., Herman, M., Buriez, J.C., Tanré, D., Bouffiès, S., Chazette, P., Roujean, J.L., 1997. Retrieval of atmospheric properties and surface bidirectional reflectances over land from POLDER/ADEOS. J. Geophys. Res. Atmos. 102, 17023–17037. https://doi.org/10.1029/96jd02662

Lewis, P & Barnsley, M., 1994. Influence of the sky radiance distribution on various formulations of the earth surface albedo. Proc. Conf. Phys. Meas. Signatures Remote Sens. 707–715.

Liang, S., 2003. A direct algorithm for estimating land surface broadband albedos from MODIS imagery. IEEE Trans. Geosci. Remote Sens. 41, 136–145. https://doi.org/10.1109/TGRS.2002.807751

Liang, S., 2001. Narrowband to broadband conversions of land surface albedo I Algorithms. Remote Sens. Environ. 76, 213–238. https://doi.org/10.1016/S0034-4257(00)00205-4

Liang, S., Shuey, C.J., Russ, A.L., Fang, H., Chen, M., Walthall, C.L., Daughtry, C.S.T., Hunt, R., 2003. Narrowband to broadband conversions of land surface albedo: II. Validation. Remote Sens. Environ. 84, 25–41. https://doi.org/10.1016/S0034-4257(02)00068-8

Los, S.O., North, P.R.J., Grey, W.M.F., Barnsley, M.J., 2005. A method to convert AVHRR Normalized Difference Vegetation Index time series to a standard viewing and illumination geometry. Remote Sens. Environ. 99, 400–411. https://doi.org/10.1016/j.rse.2005.08.017

Lucht, W., Lewis, P., 2000. Theoretical noise sensitivity of BRDF and albedo retrieval from the EOS-MODIS and MISR sensors with respect to angular sampling. Int. J. Remote Sens. 21, 81–98. https://doi.org/10.1080/014311600211000

Lucht, W., Schaaf, C.B., Strahler, A.H., 2000. An algorithm for the retrieval of albedo from space using semiempirical BRDF models. IEEE Trans. Geosci. Remote Sens. 38, 977–998. https://doi.org/10.1109/36.841980

Mayr, S., Kuenzer, C., Gessner, U., Klein, I., Rutzinger, M., 2019. Validation of Earth Observation Time-Series: A Review for Large-Area and Temporally Dense Land Surface Products. Remote Sens. 11, 2616. https://doi.org/10.3390/rs11222616

Mecklenburg, S., Dransfeld, S., Gascon, F., Nieke, J., Donlon, C., Drusch, M., Schüttemeyer, D., Berruti, B., 2018. ESA's sentinel-3 mission - Status and performance. Int. Geosci. Remote Sens. Symp. 2018-July, 3917–3919. https://doi.org/10.1109/IGARSS.2018.8518877

Meerdink, S.K., Hook, S.J., Roberts, D.A., Abbott, E.A., 2019. The ECOSTRESS spectral library version 1.0. Remote Sens. Environ. 230, 111196. https://doi.org/10.1016/j.rse.2019.05.015

Muller, J.-P., Lewis, Philip, Fischer, Jurgen, North, P., Framer, U., López, G., Kennedy, T., Lewis, Philip, Fischer, Jürgen, Guanter, L., Preusker, R., Heckel, A., Krämer, U., Danne, O., Brockmann, C., Lewis, P, 2011. The ESA GlobAlbedo Project for mapping the Earth's land surface albedo for 15 years from European sensors, Geophysical Research Abstracts.

Nicodemus, F., Richmond, J., Hsia, J., Ginsberg, I., Limperis, T., 1977. Geometrical Considerations and Nomenclature for Reflectance. Technical Report October, National Bureau of Standards, U.S. Department 333 of Commerce,Washington, DC.

Nightingale, J., Mittaz, J.P.D., Douglas, S., Dee, D., Ryder, J., Taylor, M., Old, C., Dieval, C., Fouron, C., Duveau, G., Merchant, C., 2019. Ten Priority Science Gaps in Assessing Climate Data Record Quality. Remote Sens. 11, 986. https://doi.org/10.3390/rs11080986

Nightingale, T., 2017. Sentinel-3 SLSTR PFM FPA Spectral Calibration Report [WWW Document]. URL https://sentinel.esa.int/documents/247904/3347387/Sentinel-3-SLSTR-Spectral-Calibration-Report (accessed

5.2.22).

Nightingale, T., 2015. Sentinel-3 SLSTR B FPA Spectral Calibration Report [WWW Document]. URL https://sentinel.esa.int/documents/247904/322305/SLSTR+Spectral+Calibration+Function (accessed 5.2.22).

Ollinger, S. V., Richardson, A.D., Martin, M.E., Hollinger, D.Y., Frolking, S.E., Reich, P.B., Plourde, L.C., Katul, G.G., Munger, J.W., Oren, R., Smith, M.L., Paw U, K.T., Bolsta, P. V., Cook, B.D., Day, M.C., Martin, T.A., Monson, R.K., Schmid, H.P., 2008. Canopy nitrogen, carbon assimilation, and albedo in temperate and boreal forests: Functional relations and potential climate feedbacks. Proc. Natl. Acad. Sci. U. S. A. 105, 19336–19341. https://doi.org/10.1073/PNAS.0810021105/SUPPL_FILE/0810021105SI.PDF

PDGS, 2016. GSC Sentinel-3 PDGS Products Definition - Sentinel Online [WWW Document]. URL https://sentinel.esa.int/documents/247904/351187/GSC_Sentinel-3_Products_Definition (accessed 5.2.22).

Pinty, B., Roveda, F., Verstraete, M.M., Gobron, N., Govaerts, Y., Martonchik, J. V., Diner, D.J., Kahn, R.A., 2000a. Surface albedo retrieval from Meteosat 1. Theory. J. Geophys. Res. Atmos. 105, 18099–18112. https://doi.org/10.1029/2000JD900113

Pinty, B., Roveda, F., Verstraete, M.M., Gobron, N., Govaerts, Y., Martonchik, J. V., Diner, D.J., Kahn, R.A., 2000b. Surface albedo retrieval from Meteosat: 2. Applications. J. Geophys. Res. Atmos. 105, 18113–18134. https://doi.org/10.1029/2000JD900114

Pokrovsky, I., Pokrovsky, O., Roujean, J.L., 2003. Development of an operational procedure to estimate surface albedo from the SEVIRI/MSG observing system by using POLDER BRDF measurements II. Comparison of several inversion techniques and uncertainty in albedo estimates. Remote Sens. Environ. 87, 215–242. https://doi.org/10.1016/S0034-4257(03)00166-4

Quaife, T., Lewis, P., 2010. Temporal constraints on linear BRDF model parameters. IEEE Trans. Geosci. Remote Sens. 48, 2445–2450. https://doi.org/10.1109/TGRS.2009.2038901

Rahman, H., Dedieu, G., 1994. SMAC: a simplified method for the atmospheric correction of satellite measurements in the solar spectrum. Int. J. Remote Sens. 15, 123–143. https://doi.org/10.1080/01431169408954055

Ramon, D., Jolivet, D., Compiègne, M., 2021. "CGLOPS-1" Framework Service Contract N° 199494 (JRC). Algorithm Theoretical Basis Document Atmospheric Correction for Sentinel-3 OLCI and SLSTR products. Version 1.0 Issue I1.20 [WWW Document]. URL https://land.copernicus.eu/global/sites/cgls.vito.be/files/products/CGLOPS1_ATBD_S3-AC-V1_I1.20.pdf (accessed 5.2.22).

Román, M.O., Schaaf, C.B., Lewis, P., Gao, F., Anderson, G.P., Privette, J.L., Strahler, A.H., Woodcock, C.E., Barnsley, M., 2010. Assessing the coupling between surface albedo derived from MODIS and the fraction of diffuse skylight over spatially-characterized landscapes. Remote Sens. Environ. 114, 738–760. https://doi.org/10.1016/j.rse.2009.11.014

Román, M.O., Schaaf, C.B., Woodcock, C.E., Strahler, A.H., Yang, X., Braswell, R.H., Curtis, P.S., Davis, K.J., Dragoni, D., Goulden, M.L., Gu, L., Hollinger, D.Y., Kolb, T.E., Meyers, T.P., Munger, J.W., Privette, J.L., Richardson, A.D., Wilson, T.B., Wofsy, S.C., 2009. The MODIS (Collection V005) BRDF/albedo product: Assessment of spatial representativeness over forested landscapes. Remote Sens. Environ. 113, 2476–2498. https://doi.org/10.1016/j.rse.2009.07.009

Roujean, J.-L., Leroy, M., Deschamps, P.-Y., 1992. A bidirectional reflectance model of the Earth's surface for the correction of remote sensing data. J. Geophys. Res. 97, 20455. https://doi.org/10.1029/92JD01411

Roujean, J.L., 2017. Inversion of lumped parameters using BRDF kernels, in: Comprehensive Remote Sensing. Elsevier, pp. 23–34. https://doi.org/10.1016/B978-0-12-409548-9.10346-X

Roujean, J.L., Leon-Tavares, J., Smets, B., Claes, P., Camacho De Coca, F., Sanchez-Zapero, J., 2018. Surface albedo and toc-r 300 m products from PROBA-V instrument in the framework of Copernicus Global Land Service. Remote Sens. Environ. 215, 57–73. https://doi.org/10.1016/j.rse.2018.05.015

Roy, D.P., Zhang, H.K., Ju, J., Gomez-Dans, J.L., Lewis, P.E., Schaaf, C.B., Sun, Q., Li, J., Huang, H., Kovalskyy, V., 2016. A general method to normalize Landsat reflectance data to nadir BRDF adjusted reflectance. Remote Sens. Environ. 176, 255–271. https://doi.org/10.1016/j.rse.2016.01.023

S3_MPC, 2021a. Sentinel-3 SLSTR Product Data Format Specification - Level 1 products - Sentinel Online [WWW Document]. URL https://sentinels.copernicus.eu/web/sentinel/user-guides/sentinel-3-slstr/document-library/-/asset_publisher/fgeRuiak1n39/content/id/3402065 (accessed 5.2.22).

S3_MPC, 2021b. Sentinel-3 Optical Annual Performance Report - 2020 - Sentinel Online [WWW Document]. URL https://sentinels.copernicus.eu/web/sentinel/user-guides/sentinel-3-olci/document-library/-/asset_publisher/hkf7sg9Ny1d5/content/sentinel-3-optical-annual-performance-report-2020 (accessed 5.2.22).

S3_MPC, 2019. Sentinel-3 OLCI Product Data Format Specification - Level 1 products - Sentinel Online [WWW Document]. URL https://sentinels.copernicus.eu/web/sentinel/user-guides/sentinel-3-olci/document-library/-/asset_publisher/hkf7sg9Ny1d5/content/id/3402015?_com_liferay_asset_publisher_web_portlet_AssetPublisherPortlet_INSTANCE_hkf7sg9Ny1d5_redirect=https%3A%2F%2Fsentine (accessed 5.2.22).

S3 CalVal Team, 2016a. Technical Note: Sentinel-3 OLCI-A spectral response functions [WWW Document]. URL https://sentinels.copernicus.eu/documents/247904/2700436/Sentinel-3-OLCI-A-spectral-response-functions (accessed 5.2.22).

S3 CalVal Team, 2016b. Technical Note: Sentinel-3 OLCI-B spectral response functions from pre-flight characterisation [WWW Document]. URL https://sentinels.copernicus.eu/documents/247904/2700436/Sentinel-3-OLCI-B-spectral-response-functions (accessed 5.2.22).

Samain, O., Geiger, B., Roujean, J.L., 2006. Spectral normalization and fusion of optical sensors for the retrieval of BRDF and albedo: Application to VEGETATION, MODIS, and MERIS data sets. IEEE Trans. Geosci. Remote Sens. 44, 3166–3178. https://doi.org/10.1109/TGRS.2006.879545

Sánchez-Zapero, J., Camacho, F., 2019. Product Quality Assessment Report (PQAR) of CDR and ICDR Surface Albedo v1.0 based on PROBA-V (Official reference number service contract: 2018/C3S_312b_Lot5_VITO/SC1). [WWW Document]. URL https://cds.climate.copernicus.eu/cdsapp#!/dataset/satellite-albedo?tab=doc (accessed 4.9.22).

Sanchez-Zapero, J., Camacho, F., Leon-Tavares, J., Martinez-Sanchez, E., Gorrono, J., Benhadj, I., Tote, C., Swinnen, E., Munoz-Sabater, J., 2021. Prototype for Surface Albedo Retrieval Based on Sentinel-3 OLCI and SLSTR Data in the Framework of Copernicus Climate Change. 2021 IEEE Int. Geosci. Remote Sens. Symp. IGARSS 2377–2380. https://doi.org/10.1109/IGARSS47720.2021.9555099

Sánchez-Zapero, J., Camacho, F., Martínez-Sánchez, E., Lacaze, R., Carrer, D., Pinault, F., Benhadj, I., Muñoz-Sabater, J., 2020. Quality Assessment of PROBA-V Surface Albedo V1 for the Continuity of the Copernicus Climate Change Service. Remote Sens. 2020, Vol. 12, Page 2596 12, 2596. https://doi.org/10.3390/rs12162596

Sánchez-Zapero, J., Gorroño, J., Martínez-Sánchez, E., Camacho, F., Leon-Tavares, J., Benhadj, I., Toté, C., 2021a. Algorithm Theoretical Basis Document CDR/ICDR Sentinel-3 Surface Albedo v3.0. Official reference number service contract: 2020/ COP_059_VITO_Albedo. [WWW Document]. URL https://datastore.copernicus-climate.eu/documents/satellite-albedo/C3S_COP_059_D-02_ATBD_CDR-ICDR_SA_SENTINEL3_v3.0_PRODUCTS_v1.1.pdf (accessed 5.2.22).

Sánchez-Zapero, J., Martínez-Sánchez, E., Camacho, F., 2021b. Copernicus Global Land Operations “Vegetation and Energy”. “CGLOPS-1” Framework Service Contract N° 199494 (JRC) Quality Assessment Report Sentinel-3 Top Of Canopy (TOC) reflectance Collection 300m Version 1 Issue 1.00 [WWW Document]. URL https://land.copernicus.eu/global/sites/cgls.vito.be/files/products/CGLOPS1_QAR_S3-TOCr300m-v1_I1.00.pdf (accessed 5.2.22).

Schaaf, C., Wang, Z., 2015. MCD43A3 MODIS/Terra+Aqua BRDF/Albedo Daily L3 Global - 500m V006 [Data set]. NASA EOSDIS Land Processes DAAC. [WWW Document]. USGS. https://doi.org/10.5067/MODIS

Schaaf, C.B., Gao, F., Strahler, A.H., Lucht, W., Li, X., Tsang, T., Strugnell, N.C., Zhang, X., Jin, Y., Muller, J.P., Lewis, P., Barnsley, M., Hobson, P., Disney, M., Roberts, G., Dunderdale, M., Doll, C., D’Entremont, R.P., Hu, B., Liang, S., Privette, J.L., Roy, D., 2002. First operational BRDF, albedo nadir reflectance products from MODIS. Remote Sens. Environ. 83, 135–148. https://doi.org/10.1016/S0034-4257(02)00091-3

Schaepman-Strub, G., Schaepman, M.E., Painter, T.H., Dangel, S., Martonchik, J. V., 2006. Reflectance quantities in optical remote sensing-definitions and case studies. Remote Sens. Environ. 103, 27–42. https://doi.org/10.1016/j.rse.2006.03.002

Sellers, P.J., Meeson, B.W., Hall, F.G., Asrar, G., Murphy, R.E., Schiffer, R.A., Bretherton, F.P., Dickinson, R.E., Ellingson, R.G., Field, C.B., Huemmrich, K.F., Justice, C.O., Melack, J.M., Roulet, N.T., Schimel, D.S., Try, P.D., 1995. Remote sensing of the land surface for studies of global change: Models — algorithms — experiments. Remote Sens. Environ. 51, 3–26. https://doi.org/10.1016/0034-4257(94)00061-Q

Shuai, Y., Tuerhanjiang, L., Shao, C., Gao, F., Zhou, Y., Xie, D., Liu, T., Liang, J., Chu, N., 2020. Re-understanding of land surface albedo and related terms in satellite-based retrievals. https://doi.org/10.1080/20964471.2020.1716561 4, 45–67. https://doi.org/10.1080/20964471.2020.1716561

Stephens, G.L., O'Brien, D., Webster, P.J., Pilewski, P., Kato, S., Li, J.L., 2015. The albedo of Earth. Rev. Geophys. 53, 141–163. https://doi.org/10.1002/2014RG000449

Strahler, A.H., Muller, J.-P., Members, M.S.T., 1999. MODIS BRDF/Albedo Product: Algorithm Theoretical Basis Document Version 5.0.

Toté, C., 2020. Copernicus Global Land Operations "Vegetation and Energy". "CGLOPS-1" Evaluation Report of OLCI and SLSTR cloud, cloud shadow and snow detection. Issue I1.00 [WWW Document]. URL https://land.copernicus.eu/global/sites/cgls.vito.be/files/products/CGLOPS1_QAR_S3-CloudMask_I1.00.pdf (accessed 5.2.22).

Van Leeuwen, W.J.D., Roujean, J.L., 2002. Land surface albedo from the synergistic use of polar (EPS) and geo-stationary (MSG) observing systems: An assessment of physical uncertainties. Remote Sens. Environ. 81, 273–289. https://doi.org/10.1016/S0034-4257(02)00005-6

Verhoef, W., 1984. Light scattering by leaf layers with application to canopy reflectance modeling: The SAIL model. Remote Sens. Environ. 16, 125–141. https://doi.org/10.1016/0034-4257(84)90057-9

Vermote, E., Justice, C.O., Bréon, F.M., 2009. Towards a generalized approach for correction of the BRDF effect in MODIS directional reflectances. IEEE Trans. Geosci. Remote Sens. 47, 898–908. https://doi.org/10.1109/TGRS.2008.2005977

Vermote, E.F., Tanré, D., Deuzé, J.L., Herman, M., Morcrette, J.J., 1997. Second simulation of the satellite signal in the solar spectrum, 6s: an overview. IEEE Trans. Geosci. Remote Sens. 35, 675–686. https://doi.org/10.1109/36.581987

Wang, Z., Schaaf, C., Lattanzio, A., Carrer, D., Grant, I., Roman, M., Camacho, F., Yang, Y., Sánchez-Zapero, J., 2019. Global Surface Albedo Product Validation Best Practices Protocol. Version 1.0. In Z. Wang, J. Nickeson & M. Román (Eds.), Best Practice for Satellite Derived Land Product Validation (p. 45): Land Product Validation Subgroup (WGCV/CEOS), doi: 10.5067/DOC/C [WWW Document]. https://doi.org/doi: 10.5067/DOC/CEOSWGCV/LPV/ALBEDO.001

Wang, Z., Schaaf, C.B., Sun, Q., Shuai, Y., Román, M.O., 2018. Capturing rapid land surface dynamics with Collection V006 MODIS BRDF/NBAR/Albedo (MCD43) products. Remote Sens. Environ. 207, 50–64. https://doi.org/10.1016/j.rse.2018.02.001

Wanner, W., Li, X., Strahler, A.H., 1995. On the derivation of kernels for kernel-driven models of bidirectional reflectance. J. Geophys. Res. 100, 21077–21089. https://doi.org/10.1029/95jd02371

Annex I. Main characteristics of the 58 evaluated ground stations with availability of data during the 2018–2019 period

#	Site ID	Name	Country	Network	Land Cover	Lat	Lon
1	USA_BOND	Bondville	USA	SURFRAD	Croplands	40.052	−88.373
2	BEL_BRAD	Brasschaat	Belgium	GBOV/ICOS CEOS LPV SuperSite	Mixed Forest	51.309	4.521
3	NET_CABS	Cabauw	Netherland	BSRN	Grasslands	51.971	4.927
4	AUS_CPRM	Calperum	Australia	GBOV/ICOS CEOS LPV SuperSite	Shrublands	−34.003	140.588
5	USA_DRAK	Desert Rock	USA	GBOV	Bare Soil	36.624	−116.019
6	USA_FPRK	Fort Peck	USA	GBOV	Grasslands	48.308	−105.102
7	NAM_GOBA	Gobabeb	Namibia	GBOV /ICOS CEOS LPV SuperSite	Bare Soil	−23.561	15.042
8	USA_GCMK	Goodwin Creek	USA	GBOV	Decidous Broadleaf	34.255	−89.873
9	FRA_GRIG	Grignon	France	GBOV	Croplands	48.844	1.952
10	FRA_GUYA	Guyaflux	French Guyana	GBOV /ICOS CEOS LPV SuperSite	Evergreen Broadleaf	5.279	−52.925
11	GER_HAIN	Hainich	Germany	GBOV /ICOS CEOS LPV SuperSite	Mixed Forest	51.070	10.450
12	USA_NRFT	Niwot Ridge	USA	GBOV	Evergreen Needelleaf	40.033	−105.546
13	USA_PSUS	Rock Springs	USA	GBOV	Decidous Broadleaf	40.720	−77.931
14	USA_SFSD	Sioux Falls	USA	SURFRAD	Croplands	43.730	−96.620
15	USA_SGP	Southern Great Plains	USA	GBOV	Croplands	36.606	−97.489
16	USA_TBLN	Table Mountain	USA	GBOV	Bare soil and Rocks	40.125	−105.237
17	AUS_TUMB	Tumbarumba	Australia	GBOV/ICOS CEOS LPV SuperSite	Evergreen Broadleaf	−35.657	148.152
18	LENO	Lenoir Landing	USA	NEON	Deciduous Broadleaf	31.854	-88.161
19	TALL	Talladega National Forest	USA	NEON/ICOS CEOS LPV SuperSite	Needle-Leaf	32.950	-87.393
20	BONA	Caribou-Poker	USA	NEON	Needle-Leaf	65.154	-147.503
21	DEJU	Delta Junction	USA	NEON	Needle-Leaf	63.881	-145.751

22	HEAL	Healy	USA	NEON	Shrublands	63.876	-149.213
23	TOOL	Toolik	USA	NEON	Shrublands	68.66109	-149.37047
24	SRER	Santa Rita Experimental Range	USA	NEON	Shrublands	31.911	-110.835
25	SOAP	Soaproot Saddle	USA	NEON	Needle-Leaf	37.033	-119.262
26	TEAK	Lower Teakettle	USA	NEON	Needle-Leaf	37.006	-119.006
27	CPER	Central Plains Experimental Range	USA	NEON/ICOS CEOS LPV SuperSite	Grasslands	40.816	-104.746
28	NIWO	Niwot Ridge Mountain Research Station	USA	NEON	Needle-Leaf	40.054	-105.582
29	STER	Sterling	USA	NEON	Croplands	40.462	-103.029
30	DSNY	Disney Wilderness Preserve	USA	NEON	Croplands	28.125	-81.436
31	OSBS	Ordway-Swisher Biological Station	USA	NEON/ICOS CEOS LPV SuperSite	Needle-Leaf	29.689	-81.993
32	JERC	Jones Ecological Research Center	USA	NEON	Needle-Leaf	31.195	-84.469
33	KONA	Konza Prairie Biological Station – Relocatable	USA	NEON	Grasslands	39.110	-96.613
34	KONZ	Konza Prairie Biological Station	USA	NEON	Grasslands	39.10077	-96.56309
35	HARV	Harvard Forest	USA	NEON/ICOS CEOS LPV SuperSite	Deciduous Broadleaf	42.537	-72.173
36	BART	Barlett Experimental Forest	USA	NEON	Deciduous Broadleaf	44.064	-71.287
37	GUAN	Guanica Forest	USA	NEON/ICOS CEOS LPV SuperSite	Evergreen Broadleaf	17.970	-66.869
38	ORNL	Oak Ridge	USA	NEON/ICOS CEOS LPV SuperSite	Deciduous Broadleaf	35.964	-84.28
39	MOAB	Moab	USA	NEON/ICOS SuperSite	Shrublands	38.248	-109.388
40	MLBS	Mountain Lake Biological	USA	NEON/ICOS CEOS LPV	Deciduous Broadleaf	37.378	-80.525

		Station		SuperSite			
41	SCBI	Smithsonian Conservatory Biology Institute	USA	NEON/ICOS CEOS LPV SuperSite	Deciduous Broadleaf	38.893	-78.140
42	STEI	Steigerwaldt Land Services	USA	NEON/ICOS CEOS LPV SuperSite	Deciduous Broadleaf	45.509	-89.586
43	DE-HoH	Hones Holz	Germany	ICOS/ICOS CEOS LPV SuperSite	Deciduous Broadleaf	52.087	11.222
44	SE-Svb	Svartberget	Sweden	ICOS/ICOS CEOS LPV SuperSite	Needle-Leaf	64.256	19.775
45	FI-Hyy	Hyytiala	Finland	ICOS/ICOS CEOS LPV SuperSite	Needle-Leaf	61.847	24.295
46	DE-RuS	Selhausen Juelich	Germany	ICOS/ICOS CEOS LPV SuperSite	Croplands	50.866	6.447
47	AU_ASM*	Alice Spring Meller	Australia	TERN/ICOS CEOS LPV SuperSite	Forest	-22.283	133.249
48	AU_BOY*	Boyaginj Wandoo Woodland	Australia	TERN/ICOS CEOS LPV SuperSite	Forest	-32.477	116.939
49	AU_Cum*	Cumberland Plain	Australia	TERN/ICOS CEOS LPV SuperSite	Forest	-33.615	150.724
50	AU_DRF*	Deintree Rainforest	Australia	TERN/ICOS CEOS LPV SuperSite	Forest	-16.238	145.427
51	AU_Gin*	Gingin Banksia Woodland	Australia	TERN/ICOS CEOS LPV SuperSite	Forest	-31.376	115.713
52	AU_GWW*	Great Western Woodlands	Australia	TERN/ICOS CEOS LPV SuperSite	Forest	-30.191	120.654
53	AU_LiS*	Litchfield Savanna	Australia	TERN/ICOS CEOS LPV SuperSite	Forest	-13.179	130.795
54	AU_RCR*	Robson Creek Rainforest	Australia	TERN/ICOS CEOS LPV SuperSite	Forest	-17.117	145.630
55	AU_SPU*	Samford Peri-Urban	Australia	TERN/ICOS CEOS LPV SuperSite	Forest	-27.388	152.878
56	AU_Wrr*	Warra Tall	Australia	TERN/ICOS	Forest	-43.095	146.655

		Eucalypt		CEOS LPV SuperSite			
57	AU_WSE*	Wombat Stringbark Eucalypt	Australia	TERN/ICOS CEOS LPV SuperSite	Forest	-37.422	144.094
58	AU_WDE*	Whroo Dry Eucalypt	Australia	TERN/ICOS CEOS LPV SuperSite	Forest	-36.673	145.029

(*) sites where diffuse fraction was not available for the period under study.

Annex II. Geostatistical information of the selected sites at 1 km resolution

Note: R_{CV}, R_{SE}, R_{ST} and R_{SV} stand for relative coefficient of variation, scale requirement index, relative strength of the spatial correlation and relative proportion of structural variation. ST_{SCORE} and RAW_{SCORE} represent standard and first order scores for the spatial representativeness.

#	Site ID	Footprint(m)	Seasonal Period	R_{CV} (%)	R_{SE} (%)	R_{ST} (%)	R_{CV} (%)	ST_{SCORE}	RAW_{SCORE}
2	BEL_BRAS	505	Leaf-off	11.81	0.01	0.29	-3.38	19.36	4.23
			Leaf-on	11.99	0.06	-0.58	-16.03	10.42	4.17
3	NET_CABA	580.9	Leaf-off	11.31	0.20	-2.61	7.13	13.86	4.42
			Leaf-on	32.62	0.01	0.74	11.70	6.65	1.53
4	USA_CPRM	253	Leaf-off	-5.83	31.92	4.15	-4.62	2.72	8.58
			Leaf-on	-11.07	29.70	2.53	-3.13	2.83	4.52
8	USA_GCMK	126	Leaf-off	-17.17	24.24	2.94	10.00	2.92	2.91
			Leaf-on	30.21	24.05	-5.02	45.76	1.96	1.65
10	FRA_GUYA	732	1-Season	7.21	14.95	-1.59	1.21	5.47	6.93
11	GER_HAIN	530	Leaf-off	9.41	0.00	7.24	27.19	6.84	5.31
			Leaf-on	-6.67	0.00	2.26	7.58	18.17	7.50
12	USA_NRFT	322	Leaf-off**	-	-	-	-	-	-
			Leaf-on	-2.63	21.72	-3.30	2.81	4.06	19.03
13	USA_PSUS	126	Leaf-off	81.60	27.49	11.72	113.98	1.04	0.61
			Leaf-on	1.57	24.88	2.89	-22.24	2.96	31.82
14	USA_SFSD	126	Leaf-off	-16.59	40.51	-0.95	23.19	1.85	3.01
			Leaf-on	-20.44	35.53	1.82	13.35	2.11	2.45
16	USA_TBLN	126	1-Season	-22.36	79.12	NaN	13.11	NaN	2.24
17	AUS_TUMB	884	1-Season	18.41	0.00	0.01	7.27	11.6539	2.7152
20	BONA	240	Leaf-off**	-	-	-	-	-	-
			Leaf-on	16.61	21.70	2.05	24.31	2.78	3.01
21	DEJU	278	Leaf-off**	-	-	-	-	-	-
			Leaf-on	4.96	15.05	-1.17	28.27	3.77	10.07
24	SRER	101	Leaf-off	21.43	9.26	1.47	-0.02	5.92	2.33
			Leaf-on	20.72	14.20	1.87	4.77	4.29	2.41
25	SOAP	404	Leaf-off	-11.18	0.00	-0.90	-3.32	19.48	4.47
			Leaf-on	-15.21	0.15	-2.50	-1.17	10.58	3.29
26	TEAK	745	Leaf-off	-3.35	0.00	-0.96	-7.64	25.17	14.90
			Leaf-on	-20.48	0.00	6.85	-8.13	8.46	2.44
32	JERC	530	Leaf-off	7.01	0.00	4.74	11.34	12.99	7.13
			Leaf-on	6.82	0.04	10.21	44.92	4.83	7.33
34	KONZ	101	Leaf-off	7.63	17.19	0.37	9.14	4.37	6.55
			Leaf-on	-11.73	69.09	4.85	-14.35	1.26	4.26
35	HARV	492	Leaf-off	0.59	0.00	3.41	-3.50	40.01	84.78
			Leaf-on	-12.45	2.82	3.29	23.25	6.32	4.02

36	BART	442	Leaf-off	10.23	0.00	8.58	27.31	6.50	4.89
			Leaf-on	28.10	0.27	0.36	69.25	3.04	1.78
38	ORNL	492	Leaf-off	16.77	0.09	0.48	-5.35	13.12	2.98
			Leaf-on	91.14	0.03	6.68	107.14	1.46	0.55
40	MLBS	366	Leaf-off	-9.88	0.03	0.14	30.37	7.41	5.06
			Leaf-on	13.81	3.61	1.70	167.03	1.55	3.62
41	SCBI	657	Leaf-off	61.67	0.00	1.66	56.04	2.51	0.81
			Leaf-on	14.73	0.00	0.74	6.17	13.86	3.39
42	STEI	278	Leaf-off	10.92	0.09	6.13	29.27	6.44	4.58
			Leaf-on	47.38	0.96	14.20	98.54	1.84	1.06
43	DE-HoH	253*	Leaf-off	23.67	0.10	-0.36	18.84	6.95	2.11
			Leaf-on	-7.43	5.24	-4.59	-29.11	5.28	6.73
47	AU_ASM	146	Leaf-off	-16.55	2.35	4.84	-5.35	8.88	3.02
			Leaf-on	-16.27	4.58	-4.58	-9.66	6.78	3.07
49	AU_Cum	253*	Leaf-off	20.11	0.07	5.31	22.96	6.18	2.49
			Leaf-on	109.66	4.68	3.43	160.25	1.04	0.46
50	AU_DRF	442	Leaf-off	14.79	0.03	-3.95	3.96	13.17	3.38
			Leaf-on	18.93	0.00	8.12	39.16	4.53	2.64
52	AU_GWW	253*	Leaf-off	7.61	0.00	1.08	3.88	23.87	6.57
			Leaf-on	46.29	0.05	21.87	99.44	1.79	1.08
53	AU_Lis	505	Leaf-off	-0.07	0.00	2.14	6.42	34.74	667.25
			Leaf-on	0.74	4.30	-6.45	19.08	7.66	67.63
54	AU_RCR	505	Leaf-off	11.37	0.00	-0.05	5.34	17.90	4.40
			Leaf-on	4.64	0.00	1.27	4.56	28.67	10.77
56	AU_Wrr	1010	Leaf-off	-2.75	0.00	9.07	67.96	3.76	18.16
			Leaf-on	13.28	0.00	5.60	72.04	3.30	3.77
57	AU_WSE	379	Leaf-off	18.23	0.00	6.75	11.00	8.34	2.74
			Leaf-on	17.28	0.00	1.37	4.39	13.02	2.89

*The height of the tower was not found for the estimation of footprint. Typically values of 20 m were considered for forest sites, and 10 m for other biomes.

** Not clear high resolution images were found to evaluate representativeness in the period.

Declaration of interests

☒ The authors declare that they have no known competing financial interests or personal relationships that could have appeared to influence the work reported in this paper.

☐The authors declare the following financial interests/personal relationships which may be considered as potential competing interests:

Jorge Sánchez-Zapero